Enzyme Architecture: The Effect of Replacement and Deletion Mutations of Loop 6 on Catalysis by Triosephosphate Isomerase

Xiang Zhai,[†] Maybelle K. Go,[†] AnnMarie C. O'Donoghue,[‡] Tina L. Amyes,[†] Scott D. Pegan,[§] Yan Wang,[‖] J. Patrick Loria,[‖,⊥] Andrew D. Mesecar,[#] and John P. Richard*,[†]

[†]Department of Chemistry, University at Buffalo, Buffalo, New York 14221, United States
[‡]Department of Chemistry, Durham University, Durham DH1 3EL, U.K.
[§]Department of Pharmaceutical and Biomedical Sciences, University of Georgia, Athens, Georgia 30602, United States
[‖]Department of Chemistry, Yale University, New Haven, Connecticut 06520, United States
[⊥]Department of Chemistry and Molecular Biophysics and Biochemistry, Yale University, New Haven, Connecticut 06520, United States
[#]Departments of Biological Sciences and Chemistry, Purdue University, West Lafayette, Indiana 47907, United States

S *Supporting Information*

ABSTRACT: Two mutations of the phosphodianion gripper loop in chicken muscle triosephosphate isomerase (*c*TIM) were examined: (1) the loop deletion mutant (LDM) formed by removal of residues 170–173 [Pompliano, D. L., et al. (1990) *Biochemistry 29*, 3186–3194] and (2) the loop 6 replacement mutant (L6RM), in which the N-terminal hinge sequence of TIM from eukaryotes, 166-PXW-168 (X = L or V), is replaced by the sequence from archaea, 166-PPE-168. The X-ray crystal structure of the L6RM shows a large displacement of the side chain of

E168 from that for W168 in wild-type *c*TIM. Solution nuclear magnetic resonance data show that the L6RM results in significant chemical shift changes in loop 6 and surrounding regions, and that the binding of glycerol 3-phosphate (G3P) results in chemical shift changes for nuclei at the active site of the L6RM that are smaller than those of wild-type *c*TIM. Interactions with loop 6 of the L6RM stabilize the enediolate intermediate toward the elimination reaction catalyzed by the LDM. The LDM and L6RM result in 800000- and 23000-fold decreases, respectively, in k_{cat}/K_m for isomerization of GAP. Saturation of the LDM, but not the L6RM, by substrate and inhibitor phosphoglycolate is detected by steady-state kinetic analyses. We propose, on the basis of a comparison of X-ray crystal structures for wild-type TIM and the L6RM, that ligands bind weakly to the L6RM because a large fraction of the ligand binding energy is utilized to overcome destabilizing electrostatic interactions between the side chains of E168 and E129 that are predicted to develop in the loop-closed enzyme. Similar normalized yields of DHAP, *d*-DHAP, and *d*-GAP are formed in LDM- and L6RM-catalyzed reactions of GAP in D_2O. The smaller normalized 12–13% yield of DHAP and *d*-DHAP observed for the mutant *c*TIM-catalyzed reactions compared with the 79% yield of these products for wild-type *c*TIM suggests that these mutations impair the transfer of a proton from O-2 to O-1 at the initial enediolate phosphate intermediate. No products are detected for the LDM-catalyzed isomerization reactions in D_2O of $[1\text{-}^{13}C]GA$ and HP_i, but the L6RM-catalyzed reaction in the presence of 0.020 M dianion gives a 2% yield of the isomerization product $[2\text{-}^{13}C,2\text{-}^2H]GA$.
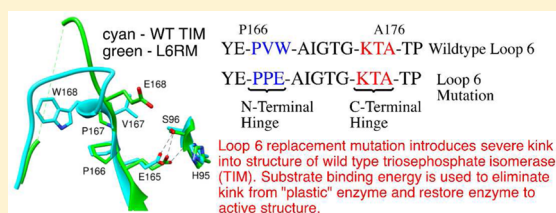
Triosephosphate isomerase (TIM) appeared early in evolution as an enzyme that catalyzes a step in glycolysis, a universal metabolic pathway.[1] TIM catalyzes the stereospecific and reversible conversion of dihydroxyacetone phosphate (DHAP) to (*R*)-glyceraldehyde 3-phosphate (GAP),[2,3] by proton transfer reactions at carbon, through enzyme-bound *cis*-enediolate reaction intermediates (Scheme 1). Intramolecular proton transfer between C-1 and C-2 is conducted by the carboxylate side chain of Glu165,[4–8] and the neutral electrophilic imidazole side chain of His-95 plays a role in mediating proton transfer between O-1 and O-2 of the enediolate.[9–11] We are interested in understanding the mechanism of action of TIM and intrigued by the repeating flexible loops at the archetypal TIM barrel.[12–15] There is a strong probability that the properties of these loops are well

adapted for catalytic strategies perfected by TIM early in evolution.[15–17] At least one strategy, the utilization of phosphodianion binding energy for catalysis,[18] has been widely observed for enzymes that catalyze a variety of reactions, including decarboxylation,[19] proton transfer,[20] hydride transfer,[21] phosphoryl transfer,[22] and a more complex reaction.[23]
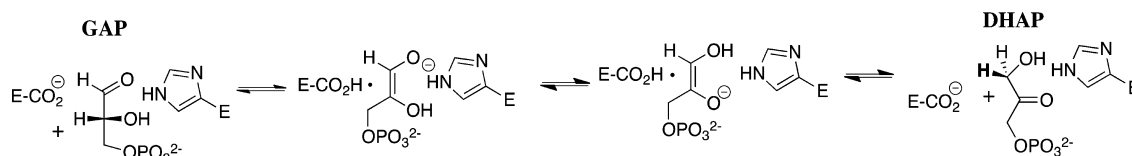
The 11-residue flexible loop 6 of TIM (Scheme 2) is open in unliganded TIM, to allow substrate free access to the active site.[14,24] Binding of DHAP to TIM triggers closure of loop 6 over the substrate phosphodianion and formation of the "caged" enzyme–PGA complex shown in Figure 1A.[15,16] The

Scheme 1

Scheme 2
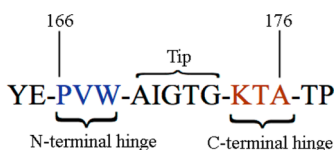

alkyl ammonium side chain of K12 stretches across the protein surface toward the base of loop 6 and forms a solvent-separated ion pair with the phosphodianion. The side chain of K12 is anchored to the protein surface by an ion pair with the carboxylate side chain of E97:[25] its deletion results in a 10^5-fold decrease in k_{cat}/K_m for the K12G mutant of TIM from yeast.[26,27] Two lines of evidence show that the interactions between loop 6 and dianions activate TIM for deprotonation of bound carbon acid substrates.

(1) Deletion of residues 170−173 from loop 6 of TIM from chicken muscle (cTIM) and introduction of a peptide bond between A169 and K174 disrupt loop−dianion interactions but should leave the protein fold unaffected (Figure 1B).[28] This loop deletion mutation (LDM) results in a 10^5-fold decrease in k_{cat}, but an only 5-fold increase in K_m for isomerization of GAP.[28] This shows that the strong stabilizing interactions between loop 6 and the ligand are expressed only at the transition state for the isomerization reaction. Interactions between loop 6 and the enediolate phosphate intermediate play the additional vital role of suppressing the breakdown of the intermediate to form methylglyoxal and inorganic phosphate,[28−30] the dominant nonenzymatic reaction of triosephosphates in water.[31]

(2) Cutting the connection between the carbon acid and phosphodianion of GAP allows the examination of the effect of TIM−dianion interactions on catalytic activity.[17,32] We have shown that the binding of phosphite dianion to TIM results in a large increase in enzymatic activity, as measured by the increase in the apparent second-order rate constant, $(k_{cat}/K_m)_{obs}$, for the TIM-catalyzed deuterium-exchange reactions of truncated substrates glycolaldehyde (GA)[32] and $[1\text{-}^{13}C]$GA in D_2O.[33] Phosphite dianion activation of enzyme-catalyzed proton transfer and decarboxylation reactions catalyzed by orotidine 5′-monophosphate decarboxylase[19,20,34,35] and for the hydride transfer reaction catalyzed by glycerol 3-phosphate dehydrogenase has also been observed.[21]

Loop 6 pivots around the N-terminal (PVW) and C-terminal (KTA) hinges during loop closure, while the "tip" residues (AIGTG) move as a rigid body (Scheme 2).[36] The loop-open and -closed forms of TIM were characterized by solid-state NMR,[37−39] solution NMR,[40,41] and temperature jump fluorescence spectroscopy studies,[42] where it was concluded that loop opening and closing is just sufficiently fast to account for TIM-catalyzed turnover of substrate. Studies of mutants at hinge residues show that substitution of glycine at these positions results in a decrease in catalytic activity.[43,44] It was proposed that the Gly mutations result in an increase in the number of protein conformations for the flexible loop-open form of TIM, which provides an entropic stabilization of the unliganded open enzyme compared with the rigid closed form of TIM.[45,46]

We report here the results of experiments on the loop 6 deletion mutant (LDM),[28] and of a loop 6 replacement mutant (L6RM), where the N-terminal hinge sequence of TIM from eukaryotes and bacteria, 166-PXW-168 (X = L or V), is
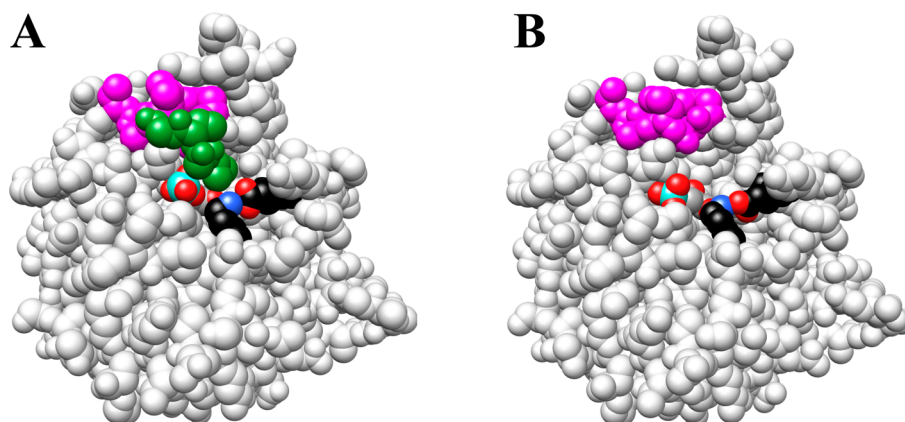

Figure 1. Models that show representations of the X-ray crystal structures of wild-type TIM and a loop 6 deletion mutant (LDM). (A) Space filling model of the complex between TIM from yeast and PGA (PDB entry 2YPI).[83] The amino acid side chains of loop 6 that were retained for the LDM are colored magenta and the deleted residues green. The cationic side chain of K12 is shown with the nitrogen (blue) in an ion pair to oxygen (red) of the anionic side chain of E97. (B) LDM of cTIM generated from the structure of wild-type cTIM by a procedure similar to that described for the K12G mutant of TIM from yeast.[26] The amino acid side chains of loop 6 that were retained for the LDM are colored magenta. Reprinted with permission from ref 17. Copyright 2012 American Chemical Society. In solution, TIM exists as a homodimer. Here we show only the monomer for the sake of clarity.

replaced with the sequence found in archaea, 166-PPE-168.[47] These include (a) steady-state kinetic and inhibition studies, (b) X-ray crystallographic and solution NMR structural data for the L6RM, (c) the products of the mutant *c*TIM-catalyzed reactions of GAP in D_2O,[48−50] and (d) kinetic and product data for the mutant TIM-catalyzed reactions of [1-^{13}C]GA in D_2O in the absence and presence of phosphite dianion.[32,33] We show that the LDM serves as a benchmark for catalysis, where there is little or no stabilization of the transition state for TIM-catalyzed isomerization by interactions with loop 6. This assists in the development of a structure-based interpretation of the effect of the L6RM on TIM-catalyzed isomerization reactions.

■ MATERIALS AND METHODS

Rabbit muscle glycerol 3-phosphate dehydrogenase and glyceraldehyde 3-phosphate dehydrogenase were purchased from Sigma. Bovine serum albumin (BSA) and protease inhibitor tablets (Complete) were purchased from Roche. DEAE-Sepharose, DEAE-Sepharose FF, and DEAE-Sephadex were from GE Healthcare. D,L-Glyceraldehyde 3-phosphate diethyl acetal (barium salt), glycerol 3-phosphate (powder), dihydroxyacetone phosphate (magnesium salt), NADH (disodium salt), dithiothreitol (DTT), Dowex 50WX4-200R, triethanolamine hydrochloride (TEA·HCl), sodium deuteroxide (40 wt %, 99.5% D), and imidazole were purchased from Sigma. NAD (free acid) was purchased from MP Biomedicals. Sodium phosphite (dibasic, pentahydrate) and sodium hydrogen arsenate (heptahydrate) were from Fluka. [1-^{13}C]-Glycolaldehyde ([1-^{13}C]GA) 99% enriched at C-1 with ^{13}C was purchased from Omicron Biochemicals as a 0.09 M solution in water. Deuterium oxide (99% D), deuterium chloride (35 wt %, 99.9% D), ^{15}NH$_4$Cl, and [^{13}C$_6$]glucose were from Cambridge Isotope Laboratories. 2-Phosphoglycolic acid was prepared by a literature procedure.[51] The disodium salt of D-glyceraldehyde 3-phosphate diethyl acetal was prepared by a literature procedure[52] and purified by column chromatography over DEAE-Sephadex. Imidazole was recrystallized from benzene. Water was from a Milli-Q Academic purification system. All other chemicals were reagent grade or better and used without further purification. The methods for the preparation of solutions and for all enzyme assays in 30 mM TEA buffer (pH 7.5) at I = 0.1 (NaCl) and 25 °C were described in a recent publication.[53]

Preparation of Enzymes. Wild-type *c*TIM was prepared as described previously,[53] using expression vector pET-15b.[33] This plasmid was introduced into the TIM-deficient *tpi*A$^-$ λDE3 lysogenic strain of *Escherichia coli*, FB215471(DE3),[53,54] and the enzyme was expressed and purified according to published procedures.[43,53] The concentration of TIM subunits was determined from the UV absorbance at 280 nm using an extinction coefficient of 33460 M^{-1} cm^{-1} that was calculated from the ProtParam tool available on the Expasy server.[55]

Loop 6 Replacement Mutant (L6RM). Expression vector pET-15b that contained the gene encoding wild-type *c*TIM was used to prepare the 167-VW-168 to 167-PE-168 mutant. The mutation was completed in a single mutagenesis step using primers 5′-GGTTCTTGCCTATGAGCCA<u>CCAGAA</u>GCTAT-CGGAACTGGTAAAACTGC-3′ (sense) and 5′-GCAGTTT-TACCAGTTCCGATAGC<u>TTCTGG</u>TGGCTCATAGGCAA-GAACC-3′ (antisense) and the wild-type plasmid as the cloning template. The sequence of the plasmid strands was confirmed by DNA sequencing. This plasmid was then introduced into the TIM-deficient *tpi*A$^-$ λDE3 lysogenic strain
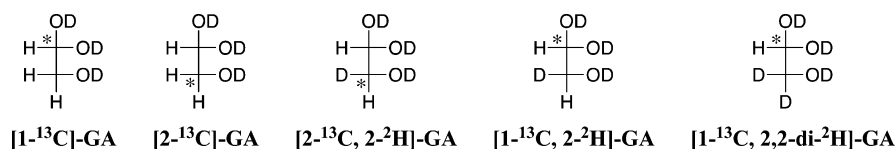
of *E. coli*, FB215471(DE3).[53] For NMR and crystallography experiments, wild-type and mutant TIM enzymes were expressed in *E. coli* BL21(DE3) cells. The loop 6 replacement mutant enzyme was expressed and purified using the procedures described for wild-type *c*TIM.[33,43] The concentration of TIM subunits was determined from the UV absorbance at 280 nm using an extinction coefficient of 27960 M^{-1} cm^{-1} that was calculated from the ProtParam tool available on the Expasy server.[55]

Loop 6 Deletion Mutant (LDM). Plasmid pBSX1cTIM, containing the wild-type gene of *c*TIM,[56] and *E. coli* strain DF502 (strep^R, tpi$^-$, and his$^-$), whose DNA lacks the gene for TIM,[57] were generous gifts from N. Sampson. The loop 6 deletion mutation was introduced into pBSX1cTIM in two steps by polymerase chain reaction mutagenesis using the QuikChange mutagenesis kit. A *Bsi*WI restriction site was first constructed by site-directed mutagenesis using the following primers to change the wild-type sense sequence from CTAT to GTAC and the antisense sequence from GATA to CATG: 5′-GTAAGGTGGTTCTTGCGTACGAGCCAGTTTGGGCTA-TC-3′ (sense) and 5′-GATAGCCCAAACTGGCTCGTACG-CAAGAACCACCTTAC-3′ (antisense). The restriction site in this plasmid, pBS09, was used to construct plasmid pBS10 for the loop 6 deletion mutant. The following primers were synthesized: 5′-GTACGAGCCAGTTTGGGCTAAAACTGC-TACTCCCCAACAGGCTCAGGAGGTTCATGAGAAGCT-GAGAGGCTGGCTCAAAAGCCAC-3′ (sense) and 5′-GTG-GCTTTTGAGCCAGCCTCTCAGCTTCTCATGAACCTC-CTGAGCCTGTTGGGGAGTAGCAGTTTTAGCCCAAAC-TGGCTC-3′ (antisense). The sense primer was complementary to bases 489−507 and 520−585 of the gene for wild-type *c*TIM and was designed to delete bases 508−519 that encode residues 170−173 of *c*TIM. The sequence of each constructed plasmid strand was confirmed by sequencing. The LDM of *c*TIM was expressed and purified by following procedures developed for wild-type *c*TIM.[33,43] The concentration of TIM subunits was determined from the UV absorbance at 280 nm using an extinction coefficient of 33460 M^{-1} cm^{-1} that was calculated from the ProtParam tool available on the Expasy server.[55]

Isotope-Labeled L6RM for NMR Studies. A sterile scraping of a plasmid glycerol stock was used to inoculate a starter culture in LB rich medium, which was grown to midlog phase. A small amount of this culture was diluted 200-fold into M9 minimal medium [0.4% (w/v) glucose] in 50% D_2O, and the cells were grown overnight. This entire culture was then transferred to 1 L of M9 minimal medium in 99% D_2O and grown to an OD$_{600}$ of 0.6−0.8, at which point 0.8 mM IPTG was added to induce protein expression at 30 °C. When necessary, uniform isotopic labeling of TIM with ^{15}N and ^{13}C was achieved using ^{15}NH$_4$Cl and [^{13}C$_6$]glucose as the nitrogen and carbon sources, respectively. Cells were harvested by centrifugation after being induced for 16−18 h and then stored frozen at −80 °C.

The frozen *E. coli* pellet was thawed on ice and then lysed by two cycles of sonication in 10 mM Tris-HCl buffer (pH 7.5) in the presence of 1 mM protease inhibitor phenylmethanesulfonyl fluoride. The lysed cell culture was clarified by centrifugation at 20000g, and Benzonase (Novagen) was added to give a final level of 25 units/mL of lysate. The crude lysate was loaded onto a DEAE-Sepharose FF weak ion-exchange column and eluted with the same buffer and a linear concentration gradient of KCl from 0 to 60 mM over a total

Chart 1

$[1\text{-}^{13}\text{C}]$-GA	$[2\text{-}^{13}\text{C}]$-GA	$[2\text{-}^{13}\text{C}, 2\text{-}^{2}\text{H}]$-GA	$[1\text{-}^{13}\text{C}, 2\text{-}^{2}\text{H}]$-GA	$[1\text{-}^{13}\text{C}, 2,2\text{-di-}^{2}\text{H}]$-GA

volume of 400 mL at a flow rate of 2 mL/min. Fractions containing cTIM were pooled and desalted using an Amicon Centriprep Concentrator with a molecular mass cutoff of 10000 kDa. The desalted sample was loaded onto the DEAE-Sepharose FF column a second time to remove minor contaminants and remaining traces of DNA. cTIM eluted from this second column in a single elution peak centered at a salt concentration of ~12 mM. The final eluted fractions containing cTIM and determined to be more than 95% pure were pooled and dialyzed against appropriate buffers, concentrated, and stored at 4 °C. The final protein yields were between 30 and 50 mg from 1 L of growth medium.

X-ray Crystal Structure Determination. The initial conditions for crystallization of the L6RM of cTIM were determined using Hampton Research Index HT, Crystal Screen HT, and SaltRx HT screens. The final crystals were grown by the hanging-drop vapor diffusion method at room temperature. The crystallization drops included 2 μL of a 35.9 mg/mL solution of the L6RM of cTIM in 10 mM 2-(N-morpholino)-ethanesulfonic acid (pH 6.60), 10 mM sodium chloride, and 0.02% sodium azide mixed in a 1:1 ratio with a precipitant of 26% PEG 3350 and 0.1 M Tris (pH 8.5). The typical crystal size was 0.1−0.2 mm.

The X-ray data set for the L6RM of cTIM was collected at SER-CAT beamline 22-ID. The crystal was mounted on nylon loops and submerged in a 5 μL volume of 30% PEG 3350 and 0.1 M Tris (pH 8.5) as a cryo solution. Crystals were subsequently flash-cooled in liquid nitrogen and mounted under a stream of dry N_2 at 100 K. The data set was collected using a MAR 300 CCD detector. X-ray images were indexed, processed, integrated, and scaled together using HKL2000.[58] The data set for the L6RM revealed a C2 space group. Initial phases were readily obtained using Phaser and wild-type cTIM (PDB entry 1TPH) as a starting model.[59] WinCoot was used for model building, and Refmac version 5.8 from the CCP4 suite was used for refinement.[60] Anisotropic temperature factors were refined, and occupancies were 1.00 for all atoms. Water molecules were added to $F_o − F_c$ density peaks that were greater than 3σ using the "Find Water" WinCoot program function. The final models were checked for structural quality using the CCP4 suite programs Procheck and Sfcheck. The atomic coordinates and structure factors have been deposited with the Protein Data Bank (PDB entry 4P61).

^{1}H NMR Product Analyses. ^{1}H NMR spectra at 500 MHz were recorded in D_2O at 25 °C using a Varian Unity Inova 500 spectrometer that was shimmed to give a line width of ≤0.7 Hz for each peak of the doublet due to the C-1 proton of GAP hydrate, or ≤0.5 Hz for the most downfield peak of the double triplet due to the C-1 proton of $[1\text{-}^{13}\text{C}]$GA hydrate. Spectra (16−64 transients) were obtained using a sweep width of 6000 Hz, a pulse angle of 90°, an acquisition time of 6 s, and a relaxation delay of 60 s ($4T_1$) for experiments on the TIM-catalyzed isomerization of GAP in D_2O or 120 s (>$8T_1$) for experiments on the TIM-catalyzed reactions of $[1\text{-}^{13}\text{C}]$GA in D_2O.[33,50] Baselines were subjected to a first-order drift correction before determination of peak areas. Chemical shifts are reported relative to HOD at 4.67 ppm.

Steady-State Kinetic Parameters. Values of k_{cat} and K_m for the LDM cTIM-catalyzed isomerization of GAP (0.075−11 mM) in solutions that contain 30 mM TEA buffer (pH 7.5) at I = 0.1 (NaCl) and 25 °C were determined from the nonlinear least-squares fit of the initial velocity data to the Michaelis−Menten equation. Arsenate (10 mM) was used as an activator for glyceraldehyde 3-phosphate dehydrogenase, the coupling enzyme in our assay for the L6RM-catalyzed isomerization of DHAP (0.08−20 mM). A control experiment showed that there is no detectable inhibition of the L6RM cTIM-catalyzed reaction by 10 mM arsenate. Inhibition of the L6RM-catalyzed reaction of GAP in the presence of 2-phosphoglycolate (PGA, 1−10 mM) was examined at pH 7.5 (I = 0.1, NaCl) by determining values of k_{cat}/K_m from the slopes of linear correlations of four or five values of $v_i/[\text{E}]$ against [GAP] for reactions at several different PGA concentrations.

Mutant cTIM-Catalyzed Isomerization of GAP in D_2O. The LDM and L6RM of cTIM were exhaustively dialyzed at 7 °C against 30 mM imidazole (70% free base) in D_2O at pD 7.9 and I = 0.1 (NaCl). The reaction in a volume of 750 μL was initiated by addition of enzyme to the reaction mixture containing GAP, imidazole buffer (pD 7.9), and NaCl in D_2O to give final concentrations of 10 mM GAP, 10 mM imidazole [70% free base; I = 0.1 (NaCl)], and 0.4 μM L6RM or 7 μM LDM. Spectra (12 transients) were recorded continuously for a period of 2−4 h, during which time >80% of GAP was converted to products. In all experiments, the fraction of the remaining substrate GAP (f_{GAP}) and the fraction of GAP converted to products DHAP (f_{DHAP}), d-DHAP ($f_{d\text{-DHAP}}$), d-GAP ($f_{d\text{-GAP}}$), and methylglyoxal (MG, f_{MG}) at time t were determined from the integrated areas of the appropriate ^{1}H NMR signals, as described previously.[50] The peak areas were normalized using the invariant signal for the C-(4,5) protons of imidazole as an internal standard.[50]

Reaction of $[1\text{-}^{13}\text{C}]$GA in D_2O. The enzymes were exhaustively dialyzed at 7 °C against 30 mM imidazole (20% free base) in D_2O at pD 7.0 and I = 0.1 (NaCl) or I = 0.024, for reactions in the absence or presence of 40 mM total phosphite, respectively. The reaction in the absence of HP$_i$ was initiated by the addition of enzyme to a mixture, which contains $[1\text{-}^{13}\text{C}]$GA, imidazole, and NaCl in D_2O, to give final concentrations of 20 mM $[1\text{-}^{13}\text{C}]$GA, 20 mM imidazole (pD 7.0, I = 0.1, NaCl), and 0.32 mM LDM or 0.39 mM L6RM of cTIM in a volume of 850 μL. The reactions in the presence of HP$_i$ at 25 °C and I = 0.1 (NaCl) were initiated by the addition of enzyme to a mixture, which contains 20 mM $[1\text{-}^{13}\text{C}]$GA, 40 mM phosphite (50% dianion, pD 7.0), 10 mM imidazole (pD 7.0), and 0.32 mM LDM of cTIM or 0.23 mM L6RM of cTIM in D_2O in a volume of 850 μL. In each case, 750 μL of the reaction mixture was transferred to an NMR tube. The NMR spectrum was recorded immediately and then at regular intervals over a period of several days. After the final spectrum had been recorded, the protein was removed by ultrafiltration

and the pD was determined. There was no significant change in pD (≤ 0.03 unit) during these reactions. The remaining reaction mixture was incubated at 25 °C and used to monitor the TIM activity. The enzymatic activity was unchanged during the time for these experiments. These reactions were monitored for the disappearance of [1-^{13}C]GA and for the formation of reaction products (Chart 1), as described previously.[33] Observed first-order rate constants, k_{obs} (s^{-1}), for the disappearance of [1-^{13}C]GA were determined from the slope of linear semilogarithmic plots of the reaction progress versus time (eq 1)

$$\ln f_s = -k_{obs}t \tag{1}$$

where f_s is the fraction of [1-^{13}C]GA that remains at time t. The observed second-order rate constant, $(k_{cat}/K_m)_{obs}$, was determined from the values of k_{obs} using eq 2

$$(k_{cat}/K_m)_{obs} = \frac{k_{obs}}{(1 - f_{hyd})[\text{TIM}]} \tag{2}$$

where f_{hyd} equals 0.94 and is the fraction of [1-^{13}C]GA present as the hydrate.[32]

NMR Analyses of Protein Structure. Concentrated stock solutions of glycerol 3-phosphate for NMR experiments were prepared gravimetrically in the same buffer used for the enzyme solutions. The pH of this stock solution was adjusted to 6.6. All NMR samples were prepared in buffer containing 10 mM MES, 10 mM NaCl, 0.02% (w/v) NaN$_3$, and 7.5% D$_2$O (pH 6.6). Samples of cTIM were labeled with ^{2}H, ^{13}C, and ^{15}N for chemical shift assignment or were uniformly (^{2}H and ^{15}N) labeled for ligand titration experiments. All NMR experiments were performed at a static magnetic field strength of 14.1 T on a Varian Inova spectrometer using a room-temperature triple-resonance probe equipped with triple-axis gradients, with the exception that the HNCA experiments were performed at a static magnetic field strength of 21.2 T at the NMR Facilities Center at the University of Colorado (Boulder, CO). Experimental temperatures were calibrated using 100% methanol as a standard. NMR data were processed in NMRPipe[61] and analyzed using Sparky.[62] Two-dimensional ^{1}H$-^{15}$N NMR experiments for all protein samples were recorded with identical parameters using spectral widths of 2400 × 8000 Hz and 256 × 2048 points in the t_1 and t_2 dimensions.

Three-dimensional backbone assignment experiments require uniformly enriched labeling of ^{15}N and ^{13}C. Resonance assignments for wild-type cTIM were obtained from those determined by J. Kempf in the Loria lab and deposited as BioMagResBank entry 15064.[45] Many resonances in mutant enzymes could be assigned by direct comparison with the wild-type ^{1}H$-^{15}$N correlation spectra. These assignments were confirmed and ambiguities resolved using data from TROSY-based HN(CA)CB[63-65] and HNCA experiments.[66]

Binding of Glycerol 3-Phosphate. Formation of the complex between G3P and wild-type cTIM was monitored at 25 °C in a series of TROSY-based ^{1}H$-^{15}$N correlation experiments. Protein samples were uniformly labeled with ^{15}N and perdeuterated. Using known assignments, the change in the chemical shift of well-resolved peaks, with an increasing G3P concentration, was monitored until ligand saturation, when the chemical shifts were not affected by further ligand addition. Chemical shift changes were quantified by eq 3

$$\delta^{NH} = \sqrt{\frac{(H_{WT} - H_{mut})^2 + (N_{WT} - N_{mut})^2/25}{2}} \tag{3}$$

in which H and N refer to the ^{1}H and ^{15}N residue specific chemical shifts, respectively, for wild-type and mutant enzymes.[67]

■ RESULTS

The genes for the 167-PE-168 loop 6 replacement mutant (L6RM) and the 170-IGTG-173 loop deletion mutant (LDM) of cTIM were expressed using different cTIM-deficient strains of *E. coli*. The LDM was expressed from *E. coli* strain DF502 (strep^R, tpi$^-$, and his$^-$),[57] while the L6RM was expressed from the *tpi*A$^-$ λDE3 lysogenic strain of *E. coli*, FB215471(DE3).[53,54] The latter strain shows more robust growth and gives the better yields of the mutant enzyme.[53] The kinetic parameters determined here for the LDM-catalyzed isomerization of GAP at 25 °C are in agreement with the kinetic parameters reported by Knowles and co-workers for reactions at 30 °C.[28]

Assignment of Backbone Amide Resonances from NMR. Three-dimensional TROSY-based triple-resonance NMR experiments were utilized to assign the backbone amide resonances in the L6RM. In addition to comparison with the assignments of wild-type cTIM,[68] TROSY-based HN(CA)CB[65] and HNCA[66] experiments were performed on the apoenzymes of L6RM cTIM. Because the backbone amide assignments are of primary interest, only the apoenzyme forms of the mutants were prepared for three-dimensional NMR assignment experiments with triple-isotope labeling. Backbone amide assignments for G3P-bound L6RM and wild-type enzymes were obtained by performing a G3P titration experiment, during which ligand binding-induced chemical shift changes were monitored.

In total, 94 and 92% of all non-proline backbone H and N resonances of the L6RM and the L6RM−G3P complex, respectively, were assigned. Assignments of the backbone amides were obtained for all of the non-proline residues in loop 6 of the L6RM (residues 166−176) and for all of the residues in loop 7 (residues 208−211), except for Gly210. The signals for the backbone amides of six residues in the L6RM, which were assigned for the apoenzyme, could not be identified for the enzyme−G3P complex, due to peak broadening or unresolved overlap with neighboring peaks.

Mutation-Induced Changes in Chemical Shifts. A comparison of wild-type and L6RM two-dimensional spectra is shown in Figure 2A. The chemical shift changes due to this mutation are quantified using eq 3 and shown in Figure 2B for each residue. The elevated values of δ^{NH} (>0.2 ppm) are mapped on the model for wild-type cTIM shown in Figure 2C. Significant changes in the chemical shift for wild-type cTIM were detected for the L6RM at residues Val161−Thr177, but the values of δ^{NH} for G171, G173, and K174 are slightly below 0.2 ppm. In loop 7, only V212 showed a δ^{NH} of >0.2 ppm. The L6RM also showed a significant δ^{NH} at helix E1 and at residues Gly128−Glu145 of helix E2 (Figure 2B).

Binding of Glycerol 3-Phosphate Monitored by NMR. To investigate the effect of the L6RM on enzyme−ligand interactions, binding of the substrate analogue G3P to wild-type cTIM and binding to the L6RM on the amide chemical shifts were compared. Titrations at 298 K were monitored by collecting a two-dimensional NMR spectrum at each titration point (Figure 3A,B). Intermediate exchange was detected at multiple residues in both wild-type cTIM and the L6RM as the
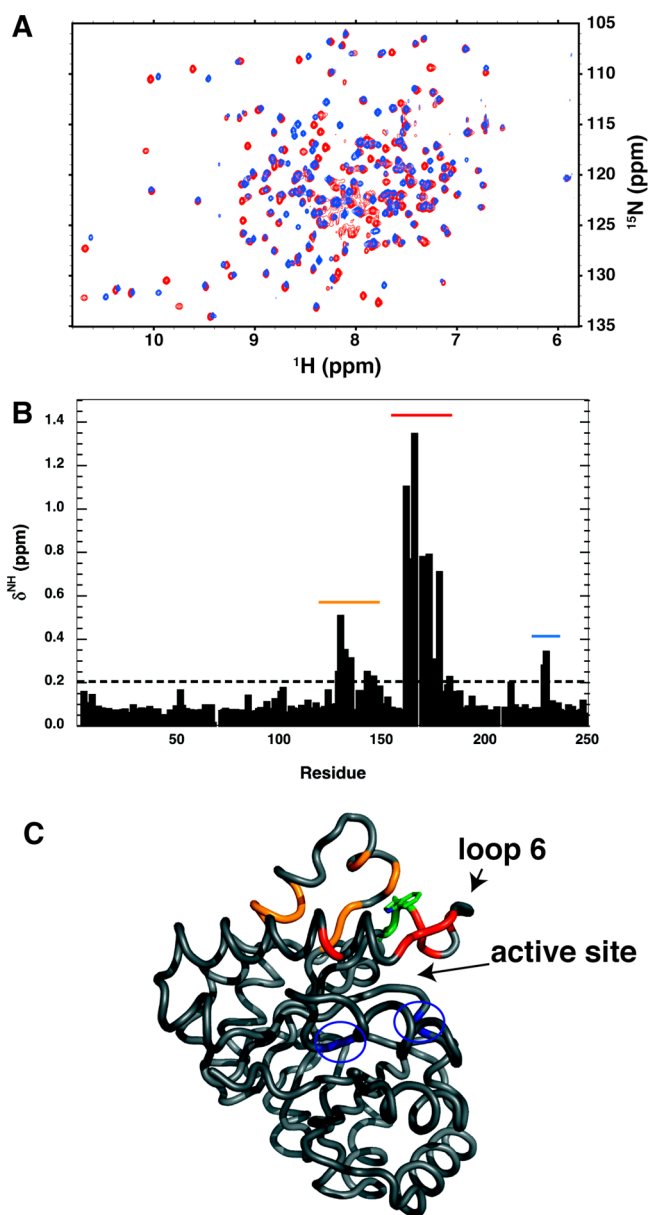
Figure 2. Summary of the effect of the L6RM on the NMR chemical shifts of backbone amide resonances, for spectra acquired at 14.1 T, 298 K, and pH 6.6. (A) Superposition of the resonances for wild-type (red) and L6RM (blue) TIM at the unliganded enzymes. (B) Values of δ^{NH} (parts per million) for the L6RM mutation, where δ^{NH} is the effect of the L6RM on the composite chemical shift, as defined by eq 3. (C) Model for wild-type cTIM, which shows the positions in the protein structure where the L6RM was found to result in significant values for δ^{NH} (>0.2 ppm). The structure has been coded to match the colors shown by the dashed line in panel B with blue residues highlighted by circles. The side chains of the two mutated residues are depicted. The positions of the active site and loop 6 are indicated to orient the viewer.

peak intensities gradually diminish as the titration end point is approached. The differences in the patterns of the residue chemical shifts for this titration indicate substantial differences between the conformations of loop 6 for the wild-type and L6RM enzymes. The final concentration of G3P in solutions of cTIM was increased to 90 and 290 mM in NMR studies of wild-type cTIM and the L6RM, respectively. Weak binding between G3P and wild-type cTIM was observed, which is

consistent with a K_i value of 1.4 mM for G3P determined for TIM from yeast.[69] The titration also shows that the binding of L6RM to G3P is significantly weaker than in wild-type cTIM.

Figure 3 illustrates the composite changes in chemical shift (δ^{NH}) upon G3P binding as a function of residue number in wild-type cTIM (Figure 3C) and the L6RM (Figure 3D). The overall averages of the values of δ^{NH} (eq 3) observed upon binding of G3P are 0.043 ± 0.050 ppm for wild-type cTIM and 0.056 ± 0.040 ppm for the L6RM, which are not significantly different. However, site specific differences in δ^{NH} induced by binding of G3P were noted for wild-type cTIM and the L6RM. Dramatic responses to G3P binding are observed in multiple regions for the wild-type enzyme, including loop 6 and loop 7, whereas in the L6RM enzyme, the ligand-induced changes in the chemical shift at loop 6 are smaller, in particular, at residues in the N-terminal portion of the loop nearest the mutations (Figure 3E,F). Other residues of wild-type cTIM, which show notable changes in chemical shift induced by the binding of G3P, include those in the vicinity of the active site such as N11, K12, H95, E97, and G232, along with neighboring residues. In the L6RM, these same residues do not experience chemical shifts of similar magnitude, indicating non-wild-type-like ligand interactions at the active site.

Steady-State Kinetics. Panels A and B of Figure 4 show the increase in $v_i/[E]$ for the L6RM-catalyzed isomerization of GAP and DHAP, respectively, in solutions that contain 30 mM TEA buffer (pH 7.5) at $I = 0.1$ (NaCl) and 25 °C. The small downward curvature in these plots is consistent with either the formation of weak Michaelis complexes with the substrate or a small decrease in k_{cat}/K_m from a specific salt effect of replacing NaCl with the substrate dianion. There is no detectable decrease in $(k_{cat}/K_m)_{obs}$ for the L6RM-catalyzed isomerization of GAP in solutions that contain 30 mM TEA buffer (pH 7.5) at $I = 0.1$ (NaCl) and 25 °C, as the concentration of the strong competitive inhibitor phosphoglycolate (PGA)[70] is increased to 10 mM (Figure S1, Supporting Information). This gives a K_i of ≥40 mM (Table 1) for inhibition by PGA, if it is assumed that a 20% decrease in k_{cat}/K_m could have been detected for the reaction at 10 mM PGA. The values of k_{cat}/K_m for L6RM-catalyzed isomerization of DHAP and DGAP (Table 1) were determined from the slopes of strictly linear portions of the Michaelis–Menten plots shown in the insets of panels A and B of Figure 4. The k_{cat}/K_m value of 470 M^{-1} s^{-1} for the L6RM-catalyzed isomerization of GAP (Table 1) and the assumption that PGA and GAP show a similar weak affinity for the L6RM (K_i, K_m ≥ 0.04 M) give a k_{cat} limit of ≥20 s^{-1} for the L6RM-catalyzed isomerization of GAP (Table 1).

Mutant cTIM-Catalyzed Isomerization of GAP in D$_2$O. The mutant cTIM-catalyzed reaction of GAP in D$_2$O was monitored by ^{1}H NMR spectroscopy, as described previously.[50] Three products form at the enzyme active site, DHAP, d-DHAP, and d-GAP, and, a fourth product, methylglyoxal, may form by nonenzymatic and enzyme-catalyzed reactions (Scheme 3).[31] The yield of each product, $(f_P)_{obs}$, was calculated from the normalized ^{1}H NMR peak area for a single proton for the particular product (A_P, eq 4) and the sum of the peak areas of single protons for all of the reaction products, as described previously.[50] The fraction of GAP remaining at a given reaction time (f_{GAP}) was calculated as the ratio of the normalized ^{1}H NMR peak area of a single proton of the remaining GAP, and the sum of the normalized ^{1}H NMR peak areas of single protons for GAP and for each reaction product.[50]
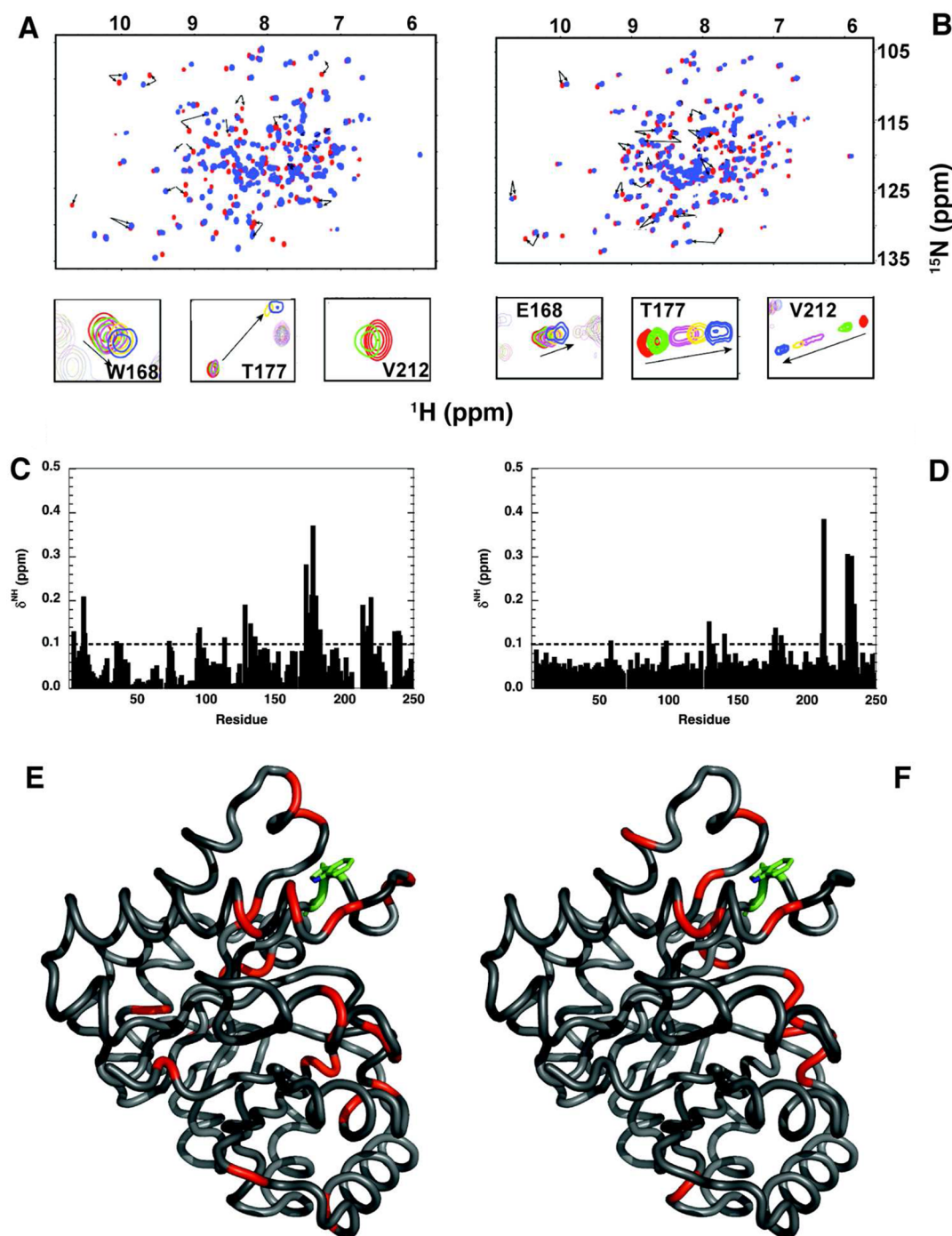
Figure 3. Summary of the effect of the binding of G3P to wild-type *c*TIM and to the L6RM on the NMR chemical shifts of backbone amide resonances, for spectra acquired at 14.1 T, 298 K, and pH 6.6. (A and B) Superposition of signals for wild-type *c*TIM (A) or the L6RM (B) in the unliganded (red) and G3P-saturated (blue) forms. The inset shows the titration profile for residues 168, 177, and 212. The arrows indicate the direction of the shift in the resonance as the unliganded enzyme is saturated by G3P. (C and D) Values of δ^{NH} (parts per million) observed upon saturation of wild-type *c*TIM (C) and the L6RM (D) by G3P, where δ^{NH} is the effect of ligand binding on the chemical shift. (E and F) Model for wild-type *c*TIM (PDB entry 1TIM), which shows, in red, the position in the protein structure where the binding of G3P results in significant values for δ^{NH} (>0.1 ppm) for wild-type *c*TIM (E) or the L6RM (F). The site of the mutation is colored green in panel F.

$$(f_p)_{obs} = A_p/(A_{DHAP} + A_{d-DHAP} + A_{d-GAP} + A_{MG}) \quad (4)$$

$$(f_{MG})_N = \frac{k_N}{k_{obs}} \quad (5)$$

$$(f_{MG})_E = (f_{MG})_{obs} - (f_{MG})_N \quad (6)$$

Figure 5A shows the decrease in f_{GAP} with time during the reaction of 10 mM GAP catalyzed by 0.4 μM L6RM *c*TIM in D_2O buffered by 10 mM imidazole (70% free base) at $I = 0.1$ (NaCl), pD 7.9, and 25 °C. The fit of the data from Figure 5A to a single-exponential decay gave a k_{obs} of 2.7×10^{-4} s^{-1} for the disappearance of GAP. Figure 5B shows the change with time in the fractional product yields $(f_P)_{obs}$ (eq 4) for DHAP,
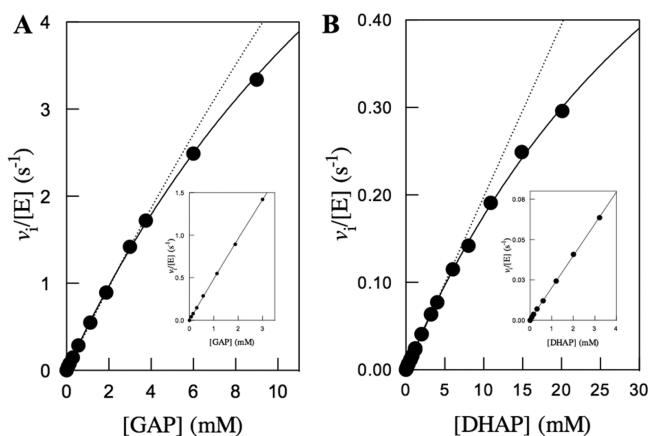
Figure 4. Michaelis–Menten plots of initial velocity data for the isomerization of GAP and DHAP catalyzed by the L6RM of *c*TIM at pH 7.5 (30 mM TEA buffer), 25 °C, and $I = 0.1$ (NaCl). The solid line shows the fit of data to the Michaelis–Menten equation, and the dashed line is the linear relationship of the data at a low substrate concentration (≤ 3 mM). The inset shows the linear correlation of the initial velocity data for ≤ 3 mM GAP or DHAP, the slope of which gives the second-order rate constant (k_{cat}/K_m).

Scheme 3

d-DHAP, and *d*-GAP during a 150 min L6RM-catalyzed reaction of GAP. The yields of DHAP, *d*-DHAP, and *d*-GAP, determined by extrapolation of the product yields (Figure 5B) to zero reaction time, are listed in Table 2. A 4% yield of MG was also observed. Combining a k_N of 1.7×10^{-5} s^{-1} determined for the nonenzymatic elimination reaction of GAP in D$_2$O at pD 7.9 (10 mM imidazole), 25 °C, and $I = 0.15$ (NaCl)[27] and a k_{obsd} of 2.7×10^{-4} s^{-1} determined from the fit of data in Figure 5A gives a theoretical yield (f_{MG})$_N$ of 0.06 (eq 5) if MG forms exclusively by nonenzymatic elimination in the presence of 0.4 μM L6RM *c*TIM in D$_2$O. This is not significantly different from the (f_{MG})$_{obs}$ of 0.04 (Table 2). We conclude that MG forms mainly or entirely by a nonenzymatic reaction.

Figure 5C shows the decrease in f_{GAP} with time during the reaction of 10 mM GAP catalyzed by 7 μM LDM *c*TIM in D$_2$O buffered by 10 mM imidazole (70% free base) at $I = 0.1$ (NaCl), pD 7.9, and 25 °C. The fit of the data from Figure 5C to a single-exponential decay gave a k_{obs} of 7.5×10^{-5} s^{-1} for the disappearance of GAP. Figure 5D shows the change with time in the fractional product yields, (f_P)$_{obs}$ (eq 4), for DHAP, *d*-DHAP, *d*-GAP, and MG during a 360 min reaction time. The yields of DHAP, *d*-DHAP, *d*-GAP, and MG determined by extrapolation of the product yields (Figure 5D) to zero reaction
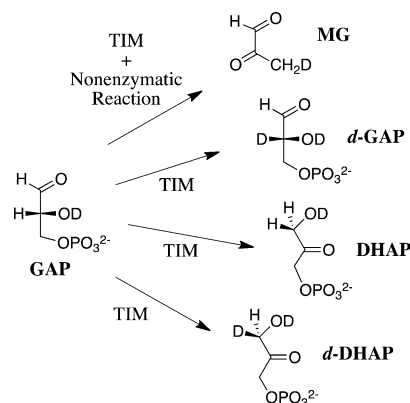
time are listed in Table 2. Table 2 also reports the normalized yield of products from proton transfer reactions at the enzyme active site, *d*-GAP, *d*-DHAP, and DHAP, calculated using eqs 7–9.

$$(f_{\text{d-GAP}})_E = \frac{f_{\text{d-GAP}}}{f_{\text{d-GAP}} + f_{\text{DHAP}} + f_{\text{d-DHAP}}} \quad (7)$$

$$(f_{\text{d-DHAP}})_E = \frac{f_{\text{d-DHAP}}}{f_{\text{d-GAP}} + f_{\text{DHAP}} + f_{\text{d-DHAP}}} \quad (8)$$

$$(f_{\text{DHAP}})_E = \frac{f_{\text{DHAP}}}{f_{\text{d-GAP}} + f_{\text{DHAP}} + f_{\text{d-DHAP}}} \quad (9)$$

Combining the k_{obs} of 7.5×10^{-5} s^{-1} for the reaction of GAP in the presence of 7 μM LDM *c*TIM and the k_N of 1.7×10^{-5} s^{-1} gives an (f_{MG})$_N$ of 0.23 (eq 5) for the fractional yield of methylglyoxal from the nonenzymatic elimination reaction (Table 2). The observed yield of MG, (f_{MG})$_{obs}$, equals 0.75, so that the yield from the LDM-catalyzed reaction, (f_{MG})$_E$, equals 0.52 (eq 6). By comparison, Knowles and co-workers reported 85 and 15% yields of MG and DHAP, respectively, from the LDM-catalyzed reaction of GAP in H$_2$O.[28]

Mutant *c*TIM-Catalyzed Reactions of [1-^{13}C]GA in D$_2$O. The following reactions of solutions of 20 mM [1-^{13}C]GA were monitored by ^{1}H NMR spectroscopy. (a) The reaction catalyzed by 0.32 mM LDM *c*TIM in 20 mM imidazole buffer at $I = 0.1$ (NaCl) and 25 °C was monitored for 140 h, during which time the loss of 60% of the total of [1-^{13}C]GA was observed. (b) The reaction catalyzed by 0.32 mM LDM *c*TIM in the presence of 40 mM phosphite (50% dianion) in 6 mM

Table 1. Kinetic Parameters for Isomerization Reactions of GAP and DHAP Catalyzed by Wild-Type *c*TIM, a Loop 6 Deletion Mutant, and a Loop 6 Replacement Mutant[a]

enzyme	substrate	k_{cat} (s^{-1})	K_m (M)	k_{cat}/K_m (M^{-1} s^{-1})	K_i (M)
wild-type[b]	GAP	3200	2.9×10^{-4}	1.1×10^7	1.9×10^{-5} PGA
	DHAP	340	5.9×10^{-4}	5.8×10^5	
L6RM[c]	GAP	>20[d]	>0.04	470	>0.04[e]
	DHAP			20	
LDM[f]	GAP	0.030 (0.045)	2.1×10^{-3} (2.3×10^{-3})	14 (20)	(1.5×10^{-3}) PGH

[a]Under standard assay conditions: 30 mM TEA buffer (pH 7.5) at $I = 0.1$ (NaCl) and 25 °C. [b]Data from ref 53. [c]Determined as the slope of the linear portion ([S] < 3 mM) of the correlations shown in panels A and B of Figure 4. [d]Calculated with the assumption that GAP and PGA show a similar weak affinity for the L6RM, by combining the lower limit of K_m (>40 mM) from the text with the k_{cat}/K_m of 470 M^{-1} s^{-1}. [e]A lower limit of K_i for PGA, calculated if 10 mM PGA caused an undetected 20% decrease in k_{cat}/K_m for the L6RM-catalyzed isomerization of GAP. [f]The kinetic parameters in parentheses are for the LDM-catalyzed isomerization at 30 °C reported in ref 28.
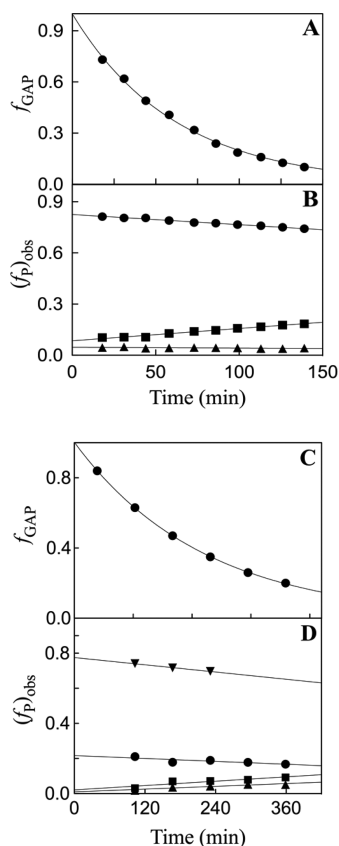
Figure 5. Rate and product data for the reactions of GAP (10 mM) in D$_2$O catalyzed by 0.4 μM L6RM cTIM (A and B) and by 7 μM LDM cTIM (C and D), determined by ^{1}H NMR spectroscopy.[50] (A and C) Decrease in the fraction of GAP (f_{GAP}) remaining for reactions catalyzed by L6RM and LDM cTIM, respectively. (B and D) Fractional product yields, $(f_P)_{obs}$ (eq 4), for reactions catalyzed by L6RM and LDM cTIM, respectively. Key for panel B: (●) $(f_{d\text{-}DGAP})_{obs}$, (■) $(f_{d\text{-}DHAP})_{obs}$, and (▲) $(f_{DHAP})_{obs}$. Key for panel D: (▼) $(f_{MG})_{obs}$, (●) $(f_{d\text{-}DGAP})_{obs}$, (■) $(f_{d\text{-}DHAP})_{obs}$, and (▲) $(f_{DHAP})_{obs}$.

Table 2. Product Distributions and Partition Rate Constant Ratios for the Reaction of GAP in D$_2$O Catalyzed by Wild-Type and Loop 6 Mutants of cTIM[a]

enzyme	k_{obs}[b] (s^{-1})	f_{DHAP}[c]	$f_{d\text{-}DHAP}$[c]	$f_{d\text{-}GAP}$[c]	$(f_{MG})_{obs}$[c]	$(f_{MG})_E$[d]
0.4 μM L6RM	2.7×10^{-4}	0.05	0.09	0.83	0.04	0
normalized product yields $(f_P)_E$[e]		0.05	0.09	0.86		
7 μM LDM	7.5×10^{-5}	0.01	0.02	0.22	0.75	0.52
normalized product yields $(f_P)_E$[e]		0.04	0.08	0.88		
				partition rate constant ratio[f]		
wild-type[g]			$(k_{C1})_H/k_{ex} = 0.96$; $(k_{C1})_D/(k_{C2})_D = 1.48$			
L6RM			$(k_{C1})_H/k_{ex} = 0.05$; $(k_{C1})_D/(k_{C2})_D = 0.10$			
LDM			$(k_{C1})_H/k_{ex} = 0.04$; $(k_{C1})_D/(k_{C2})_D = 0.09$			

[a]For the reaction of 10 mM GAP in D$_2$O buffered by 10 mM imidazole at pD 7.9 and $I = 0.10$ (NaCl). [b]Observed rate constant for the disappearance of GAP. [c]Determined by extrapolation of plots of observed normalized product yields, $(f_P)_{obs}$, vs time, to zero reaction time. [d]The difference between the observed yield of MG and the estimated yield from the nonenzymatic elimination. [e]Normalized yield of products from proton transfer reactions at the active site of TIM, calculated from the observed yields using eqs 7–9. [f]Rate constant ratios defined by eqs 11 and 12. [g]Data from ref 50.

imidazole buffer at $I = 0.1$ (NaCl) and 25 °C was monitored for 140 h, during which time the loss of 80% of the total of [1-^{13}C]GA was observed. (c) The reaction catalyzed by 0.39 mM L6RM cTIM in 20 mM imidazole buffer at $I = 0.1$ (NaCl) and 25 °C was monitored for 90 h, during which time the loss of 43% of the total of [1-^{13}C]GA was observed. (d) The reaction of [1-^{13}C]GA catalyzed by 0.23 mM L6RM cTIM in the presence of 40 mM phosphite (50% dianion) in 6 mM imidazole buffer at $I = 0.1$ (NaCl) and 25 °C was monitored for 30 h, during which time the loss of 30% of the total of [1-^{13}C]GA was observed. The observed first-order rate constant, k_{obs} (s^{-1}), for the disappearance of [1-^{13}C]GA and the observed second-order rate constant, $(k_{cat}/K_m)_{obs}$, determined as described in Materials and Methods, are listed in Table 3.

Chart 1 shows the hydrated forms of the four products of the TIM-catalyzed reaction of [1-^{13}C]GA: [2-^{13}C]GA; [2-^{13}C,2-^{2}H]GA, [1-^{13}C,2-^{2}H]GA, and [1-^{13}C,2,2-di-^{2}H]-GA.[33,53,71–73] The dideuterated product [1-^{13}C,2,2-di-^{2}H]GA forms in a nonspecific protein-catalyzed reaction.[27,33,74] Scheme 4 shows the isomerization products [2-^{13}C]GA and [2-^{13}C,2-^{2}H]GA, which form at the active site of TIM (Scheme 4), and [1-^{13}C,2-^{2}H]GA, which may form either at the enzyme active site or in a nonspecific protein-catalyzed reaction.[27,33,74] The major product of the LDM-catalyzed reaction, [1-^{13}C,2,2-di-^{2}H]GA, forms in yields of 39 and 34% for the reactions in the absence and presence of 0.020 M HP$_i$, respectively. No [2-^{13}C]GA or [2-^{13}C,2-^{2}H]GA was detected from the LDM-catalyzed reactions, but [1-^{13}C,2-^{2}H]GA forms in 10 and 15% yields for the reactions in the absence and presence of the dianion activator, respectively. The sum of the observed product yields from these slow, mainly protein-catalyzed reactions is less than 100%.[33,72,74] The other products, from the slow nonenzymatic reactions of glycolaldehyde, have not been identified.[32]

$$\frac{k_{cat}}{K_{HP_i}K_{GA}} = \left[\frac{(k_{cat}/K_m)_{obs}}{[HPO_3^{2-}]} \right] \sum (f_P)_E \tag{10}$$

The major product of the L6RM-catalyzed reactions of [1-^{13}C]GA in the absence (28% yield) and presence of 0.020 M HP$_i$ (34% yield) is [1-^{13}C,2,2-di-^{2}H]GA from a nonspecific protein-catalyzed reaction.[74] In the presence of 0.020 M HP$_i$, small yields of 0.2 and 2% of the products of isomerization at the active site, [2-^{13}C]GA and [2-^{13}C,2-^{2}H]GA, respectively, were observed, along with a 10% yield of [1-^{13}C,2-^{2}H]GA. In the absence of HP$_i$, no [2-^{13}C]GA or [2-^{13}C,2-^{2}H]GA was detected, and the yield of [1-^{13}C,2-^{2}H]GA was 7%. In both cases, the yield of [1-^{13}C,2-^{2}H]GA is similar to that for the LDM-catalyzed reactions (above), for which no products of isomerization at the enzyme active site are observed. This suggests that [1-^{13}C,2-^{2}H]GA forms mainly by nonspecific protein-catalyzed reactions of the LDM and L6RM. An approximate value of 0.5 M^{-2} s^{-1} for $(k_{cat}/K_{HP_i}K_{GA})$ was calculated for the LR6M-catalyzed reaction (Scheme 5), using eq 10, a $(k_{cat}/K_m)_{obs}$ of 0.25 M^{-1} s^{-1} (Table 3), 0.020 M HPO$_3^{2-}$, and the approximate product yield $[\sum(f_P)_E]$ of ≈0.04. This yield was estimated by assuming equal 0.02 fractional yields of deuterium-labeled products [1-^{13}C,2-^{2}H]GA and [2-^{13}C,2-^{2}H]GA from reactions of [1-^{13}C]GA at the active site of the L6RM of TIM

X-ray Crystal Structure for the L6RM. Solutions of the L6RM were screened robotically against 288 precipitant

Table 3. Kinetic Data for the Reaction of $[1\text{-}^{13}\text{C}]$GA Catalyzed by LDM and L6RM cTIM in D_2O in the Absence and Presence of HP_i[a]

enzyme	$[HPO_3^{2-}]$ (mM)	[TIM] (M)	k_{obs}[b] (s^{-1})	$(k_{cat}/K_m)_{obs}$[c] $(M^{-1}\,s^{-1})$	$k_{cat}/K_{HP_i}K_{GA}$[d] $(M^{-2}\,s^{-1})$
LDM	0	3.2×10^{-4}	2.6×10^{-6}	0.14	
	20.0	3.2×10^{-4}	4.0×10^{-6}	0.22	≤ 0.25[e]
L6RM	0	3.9×10^{-4}	2.7×10^{-6}	0.11	
	20.0	2.3×10^{-4}	3.4×10^{-6}	0.25	0.50[f]

[a]For reactions of 20 mM $[1\text{-}^{13}\text{C}]$GA in D_2O at pD 7.0 (10 mM imidazole) and $I = 0.1$ (NaCl). [b]Observed first-order rate constant for the reactions of $[1\text{-}^{13}\text{C}]$GA calculated on the basis of eq 1. [c]Second-order rate constant for the cTIM-catalyzed reactions of $[1\text{-}^{13}\text{C}]$GA calculated on the basis of eq 2. [d]The estimated third-order rate constant for the HP_i-activated cTIM-catalyzed reactions of $[1\text{-}^{13}\text{C}]$GA calculated on the basis of eq 10. [e]The upper limit for k_{cat}/K_mK_{HP}, which could have been detected in these experiments, shown as the horizontal dotted line in Figure 8. [f]Estimated as described in the text.

Scheme 4

Scheme 5

$$\frac{k_{cat}}{K_{HP_i}K_{GA}} = \left[\frac{(k_{cat}/K_m)_{obs}}{[HPO_3^{2-}]} \right] \sum (f_P)_E \qquad (10)$$
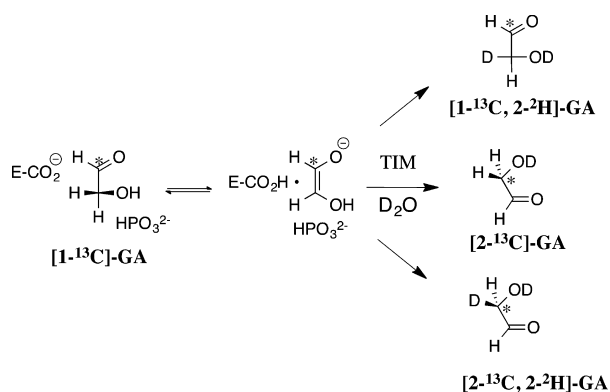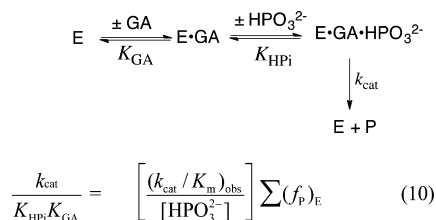
conditions from the Hampton Research's HT screens. Numerous precipitant conditions generated crystals. Ultimately, a solution containing PEG 3350 and Tris (pH 8.5) produced L6RM crystals that diffracted to 1.3 Å. Through utilization of molecular replacement, initial phase information was obtained, which yielded the structure of the L6RM as a dimer in space group C2. Data refinement and collection statistics for the L6RM crystal structure are listed in Table S1 of the Supporting Information.

The overall secondary and quaternary X-ray structure of L6RM is a TIM barrel. Gaps in the electron density in the region of loop 6 are observed for both subunits A and B, with subunit A showing the smaller gap, which runs from residue 173 to 175 (Figure S2 of the Supporting Information). A close inspection of the region containing loop 6 reveals several important differences from the structure of wild-type cTIM and of several other loop 6 mutants (PDB entries 1SU5, 1SW0, 1SW3, and 1SW7).[75] Figure 6A shows that W168 of wild-type cTIM is directed toward the protein core by a cation−π interaction[76] with the side chain of R134, and Figure 6B shows that formation of a complex with the intermediate analogue phosphoglycolohydroxamate (PGH) induces a conformational change, which replaces the cation−π interaction by a hydrogen

bond between the indole NH group and the carboxylate side chain of E129 (Figure 6B). By contrast, the better-defined structure for subunit A of the L6RM shows the carboxylate side chain of E168 displaced toward solution, compared with wild-type cTIM, probably to relieve destabilizing interactions with the side chain of E129 (Figure 6C). The structure for loop 6 in TIM from eukaryotes and bacteria is similar to that for archeal TIM,[77−79] because the equivalent N-terminal hinge residue (W168 or E147) is stabilized by functionally equivalent interactions with the protein core. This is shown by the X-ray crystal structure of TIM from *Pyrococcus woesei* (*Pw*TIM) liganded to 3-phosphonopropanoic acid, where the glutamate side chain of the 145-PPE-147 hinge interacts with the protein core through a salt bridge to the side chain of K159 (Figure 6D).

DISCUSSION

Sun and Sampson have prepared a library of 8000 mutants of the N-terminal hinge of cTIM from chicken muscle [166-XXX-168].[43,44,80] Only 3% of the library members complement a DF502 TIM-deficient strain of *E. coli* and show ≈70% of the wild-type enzyme activity.[44] Several noncomplementing members of this library were characterized, including the glycine rich 166-GGG-168 mutant, which showed a 130-fold decrease in k_{cat}/K_m.[44] These glycine mutations were proposed to result in an increase in the number of protein conformations for the loop-open form of TIM. This corresponds to the entropic stabilization of the open enzyme compared with the active rigid closed form of TIM, which results in a significant entropic price for ordering the flexible loop at the closed enzyme.[45,46]

The contributions of interactions between loop 6 and the substrate phosphodianion to catalysis by TIM were examined in this work by eliminating these interactions in the I170−G173 LDM[28] and by modifying these interactions in the L6RM. The LDM and L6RM result in large 800000- and 23000-fold decreases, respectively, in k_{cat}/K_m for isomerization of GAP. Each mutation results in a decrease in the affinity of substrates and intermediate analogues PGA and PGH for cTIM (Table 1), but the ligands bind significantly more tightly to the LDM, where there can be no stabilization of ligand by interactions with loop 6, compared with the case for the L6RM, where the loop−ligand interactions have been modified (Table 1). This shows that complexes of the L6RM are destabilized by the interaction between the ligand and modified loop 6.

X-ray Crystallographic and NMR Structural Studies. The X-ray crystallographic and NMR structural data were obtained for proteins in solutions that contain the same buffer. The crystal structure of the unliganded L6RM shows that this substitution introduces a kink into loop 6, which results in a
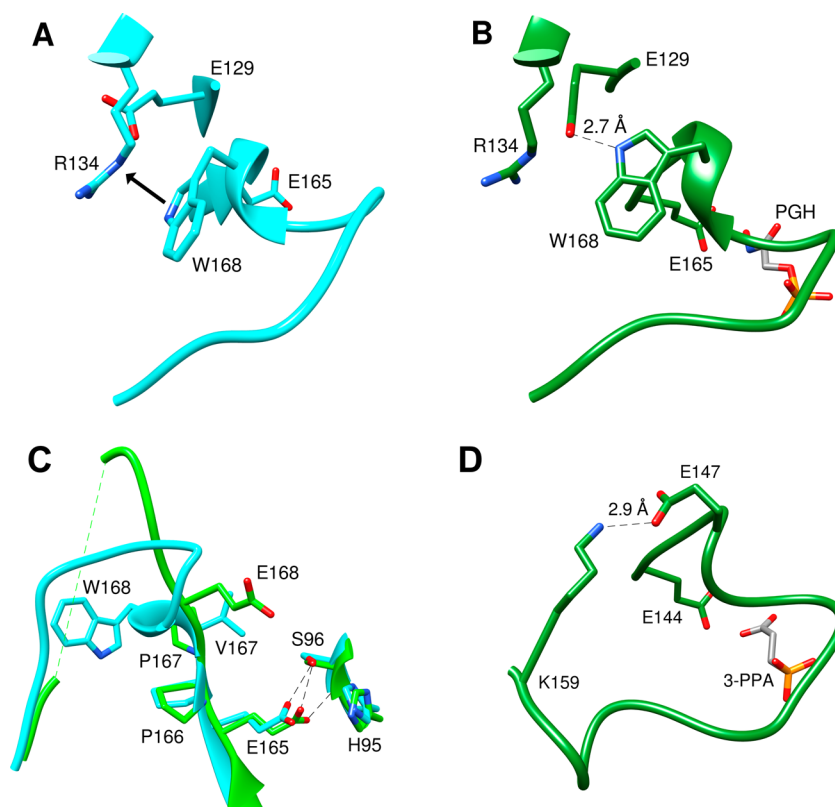
Figure 6. Representations of X-ray crystal structures of TIM in the region of the N-terminal hinge of loop 6. (A) Wild-type *c*TIM (PDB entry 1TIM). (B) Wild-type *c*TIM liganded to PGH (PDB entry 1TPH). (C) Superimposed X-ray crystal structures of unliganded *c*TIM in the region of the N-terminal hinge: blue ribbon, wild-type *c*TIM (PDB entry 1TIM); green ribbon, unliganded L6RM of *c*TIM (PDB entry 4P61). Monomer B, shown for the L6RM, has no significant electron density from residue 173 to 175. (D) TIM from *P. woesei* liganded to 3-phosphonopropanoic acid (PDB entry 1HG3). The carboxylate side chain of hinge residue E147, which occupies a position equivalent to that of W168 from *c*TIM, is stabilized by a hydrogen bond to the cationic side chain of K159.

large displacement of the carboxylate side chain of Glu168 from the position of the tryptophan side chain of W168 for the wild-type enzyme (Figure 6C). There is a smaller movement in the position of the side chains for the tip residues and a good overlap of the residues at the C-terminal hinge, and in the positions of the catalytic side chains for H95 and E165. The L6RM leads to significant changes in the chemical shifts for nuclei at loop 6 and elsewhere in the protein (Figure 2B). An NMR titration shows that G3P binds with a higher affinity to wild-type *c*TIM than to the L6RM. The binding of G3P induces significant changes in the chemical shifts for multiple nuclei in the regions of loops 6 and 7 of wild-type *c*TIM, and nuclei associated with residues 10−13, 94, and 95 (Figure 3C), but substantially smaller changes in the chemical shifts for the corresponding nuclei of the L6RM (Figure 3D). This shows that there are substantial differences in the enzyme conformational change associated with the binding of G3P to wild-type *c*TIM and the L6RM.

The LDM provides a benchmark for the catalytic properties of TIM for a case in which there is minimal enzyme activation by loop closure over the substrate phosphodianion. The differences between the kinetic parameters and products for the benchmark LDM- and L6RM-catalyzed reactions provide strong evidence that the mutant loop 6 of the L6RM plays an activating role by closing over the ligand phosphodianion at the transition state for the TIM-catalyzed isomerization reaction.

(1) The >700-fold larger value of k_{cat} for the L6RM (>20 s^{-1}) compared with that of the LDM-catalyzed (0.03 s^{-1}) isomerization of GAP (Table 1) shows that the transition state for the former reaction is stabilized by interactions with gripper loop residues.

(2) Good yields for the elimination reaction product methylglyoxal are obtained from the LDM-catalyzed reaction of GAP, because of the loss of interactions between the tip residues of loop 6 and the enediolate intermediate, which stabilize the intermediate toward elimination of inorganic phosphate.[28,31] By contrast, no products of an L6RM-catalyzed elimination reaction are observed. This provides strong evidence that there is a strong stabilization of the bound intermediate toward elimination of inorganic phosphate by interactions with loop 6.

We therefore propose that GAP and DHAP form Michaelis complexes to the L6RM, which are destabilized by interactions with the twisted loop, and that these complexes isomerize to the active loop-closed enzyme, with loop 6 positioned in a manner similar to that for wild-type *c*TIM. Interactions between TIM and the appropriate spectator dianion, such as the phosphodianion of GAP or HP$_i$, lock the enzyme into a catalytically active form that is otherwise present at low concentrations.[16,17,53,81,82] This is shown in Scheme 6, where GAP binds to form an initial nonproductive complex to TIM and the conformational change to form the active closed enzyme is favorable [$K_C \gg 1$ (Scheme 6)]. Our results provide evidence that loop closure at the Michaelis complex with the

Scheme 6

$$E_O \xrightleftharpoons{K_d} E_O{\cdot}GAP \xrightleftharpoons{K_c} E_C{\cdot}GAP \xrightarrow{k_{cat}} E \ + \ DHAP$$
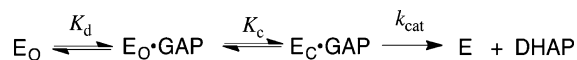
L6RM is unfavorable [$K_C \ll 1$ (Scheme 6)], because this creates destabilizing electrostatic stress between the carboxylate side chains of E168 and E129 (Figure 6B). The weak binding of the ligand to the L6RM shows that there is a large energetic price for removing the kink in loop 6, as this loop closes over the ligand dianion. Consequently, a large fraction of the intrinsic ligand binding energy is utilized to drive the enzyme conformational change, so that little binding energy is available to stabilize the Michaelis complex. These results are consistent with a malleable protein structure for TIM where the effect of mutations such as the L6RM, which distort the protein structure, may be overcome by utilization of the phosphodian-ion binding energy available to mold the enzyme into the catalytically active loop-closed conformation.

Partitioning of the Reaction Intermediate. Table 2 reports the products of the partitioning of the enediolate intermediate of the reaction of h-GAP in D_2O. These product yields define the macroscopic rate constant ratio $(k_{C1})_H/k_{ex}$ (eq 11) for partitioning of the intermediate labeled with -H at the carboxylic acid side chain of Glu165, between exchange of the -H for the -D from solvent to give deuterium-labeled products, and transfer of -H to C-1 of the intermediate to form DHAP, and $(k_{C1})_D/(k_{C2})_D$ (eq 12) for partitioning of the enediolate intermediate labeled with -D at the carboxylic acid side chain of

Glu165 between hydron transfer to C-1 and C-2 to form d-DHAP and d-GAP, respectively.

$$\frac{(k_{C1})_H}{k_{ex}} = \frac{[DHAP]}{[d\text{-DHAP}] + [d\text{-GAP}]} \tag{11}$$

$$\frac{(k_{C1})_D}{(k_{C2})_D} = \frac{[d\text{-DHAP}]}{[d\text{-GAP}]} \tag{12}$$

The rate constant ratios $(k_{C1})_H/k_{ex} = 0.04$ and 0.05 and $(k_{C1})_D/(k_{C2})_D = 0.09$ and 0.10 determined for partitioning of the enediolate phosphate intermediates of the LDM- and L6RM-catalyzed reactions, respectively, of GAP in D_2O are remarkably similar to one another, but different from the ratios of $(k_{C1})_H/k_{ex} = 0.96$ and $(k_{C1})_H/k_{ex} = 1.48$ determined for wild-type cTIM (Table 2).[50] We conclude that these mutations result in a decrease in the velocity of formation of h-DHAP relative to the rate of exchange of -H-labeled TIM with deuterium from solvent, and in the rate of formation of d-DHAP relative to the rate of formation of d-DGAP (Figure 7). Formation of both h-DHAP and d-DHAP requires hydron migration from O-2 to O-1 of the enediolate phosphate generated by deprotonation of GAP that is facilitated by the imidazole side chain of His95 (Figure 7).[11] Our results suggest that hydron migration between O-2 and O-1 is relatively fast and supports efficient wild-type cTIM-catalyzed isomerization but that this migration is impaired at the LDM and L6RM, so that internal return of the O-2-protonated enediolate phosphate to h-GAP and d-GAP is favored. The result is that a larger
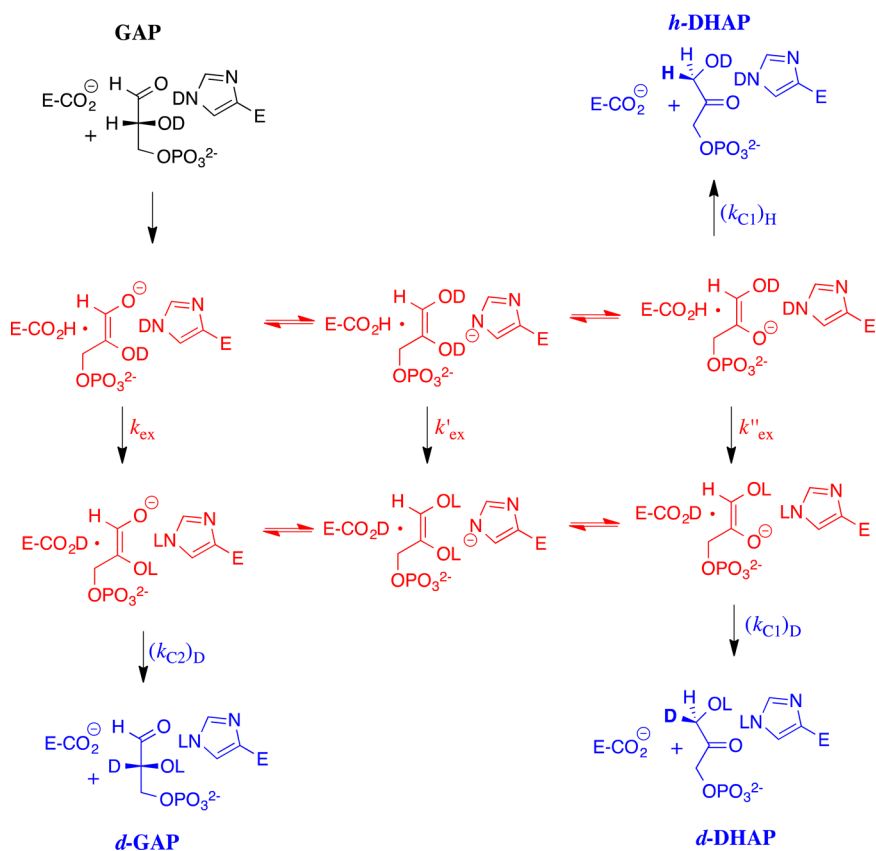

Figure 7. Scheme showing the minimal mechanism for the TIM-catalyzed reactions of GAP in D_2O that results in the formation of h-DHAP, d-DHAP, and d-GAP. The -H derived from the substrate may exchange with a pool of deuterium at the enzyme. There is evidence that the transfer of hydrogen between O-1 and O-2 of the enediolate reaction intermediate is mediated by the imidazole side chain of His95.[11]

fraction of substrate deprotonation steps are nonproductive and result in either "hidden" internal return to regenerate h-GAP or the formation of d-GAP. The fast washout of hydrogen from the active sites of the LDM and L6RM, to give a 95−96% yield of deuterium-labeled product, may also reflect an increase in the accessibility of the active site to bulk solvent.

Dianion Activation of cTIM-Catalyzed Reactions of [1-^{13}C]GA. The major products of the LDM- and L6RM-catalyzed reactions are [1-^{13}C,2,2-di-^{2}H]GA (30%) from a nonspecific protein-catalyzed reaction and [1-^{13}C,2-^{2}H]GA (10%) that may form either from an exchange reaction at the active site of TIM or from a nonspecific protein-catalyzed reaction.[33,72,74] No [2-^{13}C]GA or [2-^{13}C,2-^{2}H]GA is observed from the LDM-catalyzed reactions of [1-^{13}C]GA in the absence or presence of 20 mM HP$_i$, but the L6RM cTIM-catalyzed reaction of [1-^{13}C]GA gives yields of 0.2 and 2% for [2-^{13}C]GA and [2-^{13}C,2-^{2}H]GA, respectively, from formal isomerization reactions at the enzyme active site. We conclude that the L6RM shows barely detectable activation by HP$_i$. We estimate a $k_{cat}/K_{GA}K_{HP_i}$ value of ≈0.5 M^{-2} s^{-1} (eq 10 for Scheme 5) for the reaction activated by 20 mM phosphite dianion (Results) but that this rate constant is not significantly different from 0 for the LDM.

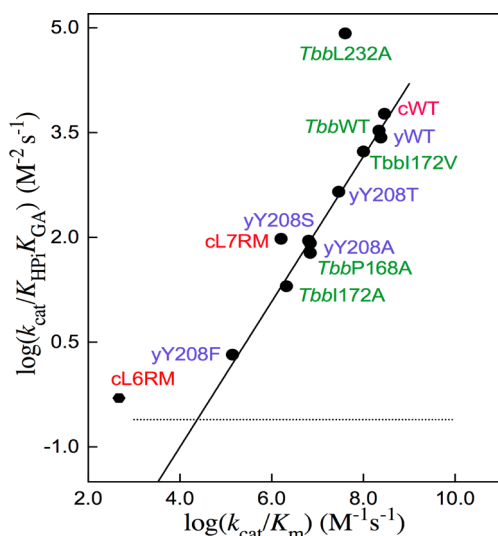Figure 8 shows the recently reported linear free energy relationship, with a slope of 1.04 ± 0.03, between values of

Figure 8. Linear free energy relationship, with a slope of 1.04 ± 0.03, between logarithmic values of second-order rate constants [log(k_{cat}/K_m)$_{GAP}$] for wild-type and mutant TIM-catalyzed isomerization of GAP and the third-order rate constants [log($k_{cat}/K_{HP_i}K_{GA}$)] for wild-type and mutant TIM-catalyzed reactions of the substrate pieces GA and HP$_i$ (Scheme 5). Most of these data were reported and discussed in an earlier publication.[82] The dotted line shows an estimate for the smallest third-order rate constant ($k_{cat}/K_{HP_i}K_{GA}$) that could have been detected by our experimental methods. Key for mutants of TIM: green for TIM from *Trypanosoma brucei*, red for TIM from chicken muscle, and blue for TIM from yeast.

log(k_{cat}/K_m)$_{GAP}$ for wild-type and mutant TIM-catalyzed reactions of (R)-GAP and log($k_{cat}/K_{HP_i}K_{GA}$) for reactions of the substrate pieces glycolaldehyde and HP$_i$ (Scheme 5).[82] The horizontal dotted line is drawn for the estimated limiting rate constant ($k_{cat}/K_{HP_i}K_{GA}$) of 0.25 M^{-2} s^{-1} for activation by 0.020

M HP$_i$, assuming (k_{cat}/K_m)$_{obs}$ = 0.25 M^{-1} s^{-1} (Table 3) and that the yield of the products of the specific TIM-catalyzed reactions is $\sum(f_P)_E$ < 0.02 (eq 10), which would be difficult or impossible to detect by our methods. This limiting rate constant is approached for mutant forms of TIM as (k_{cat}/K_m)$_{GAP}$ approaches 10^4 M^{-1} s^{-1}. By comparison, (k_{cat}/K_m)$_{GAP}$ values of 470 and 14 M^{-1} s^{-1} were determined for the L6RM and the LDM, respectively. The $k_{cat}/K_{HP_i}K_{GA}$ value of 0.5 M^{-2} s^{-1} estimated for the L6RM shows a positive deviation from the linear correlation in Figure 8, and a similar positive deviation has been reported for the loop 7 replacement mutant of cTIM.[53,82] We conclude that the failure to observe activation of the LDM by phosphite dianion is as expected for the 800000-fold smaller value of (k_{cat}/K_m)$_{GAP}$ for the LDM, compared with the value for wild-type cTIM-catalyzed reactions. These results are consistent with the conclusion that a functioning loop 6 is required to observe dianion activation of TIM for catalysis of deprotonation of bound substrate, but they do not definitively exclude the possibility of weak dianion activation of reactions catalyzed by the LDM.

■ CONCLUSIONS

The results reported here are consistent with the requirement that TIM undergo an energetically uphill change in conformation from an inactive open conformation to an active closed form, which is driven by the intrinsic phosphodianion binding energy.[16,17,33,53,71] Catalysis by the L6RM provides a remarkable example of the plasticity of the structure of cTIM. We find that the severe distortion in the structure of the unliganded wild-type enzyme (Figure 6C) may be overcome by the utilization of phosphodianion binding energy to mold cTIM into the catalytically active closed form. The observed binding of the substrate dianion to the L6RM is consequently much weaker than for wild-type TIM. By contrast, there is compelling evidence that the L232A mutation of TIM from *Trypanosoma brucei* reduces the barrier for the phosphodianion-driven conformational change.[71,73] The result of this reduced barrier to formation of the catalytically active enzyme is that a larger fraction of the total dianion binding energy is expressed at Michaelis complexes with GAP, DHAP, and HP$_i$.[71,73]

■ ASSOCIATED CONTENT

Ⓢ Supporting Information
Statistics from X-ray data collection and refinement for the X-ray crystal structure of the L6RM (Table S1), dependence of the apparent second-order rate constant, (k_{cat}/K_m)$_{app}$, for the isomerization of GAP, catalyzed by the L6RM of cTIM, on the concentration of PGA (Figure S1), and a figure that shows the electron density in the region of loop 6 for subunit A of the L6RM of cTIM (Figure S2). This material is available free of charge via the Internet at http://pubs.acs.org.

■ AUTHOR INFORMATION

Corresponding Author
*E-mail: jrichard@buffalo.edu. Telephone: (716) 645-4232. Fax: (716) 645-6963.

Notes
The authors declare no competing financial interest.

■ ACKNOWLEDGMENTS

■ ABBREVIATIONS

TIM, triosephosphate isomerase; cTIM, triosephosphate isomerase from chicken muscle; DHAP, dihydroxyacetone phosphate; GAP, (R)-glyceraldehyde 3-phosphate; d-DHAP, $[1(R)\text{-}^2H]$dihydroxyacetone phosphate; d-GAP, $[2(R)\text{-}^2H]$-glyceraldehyde 3-phosphate; TEA, triethanolamine; MES, 2-(N-morpholino)ethanesulfonic acid; MG, methylglyoxal; GA, glycolaldehyde; PDB, Protein Data Bank; PGA, 2-phosphoglycolate; HP$_i$, phosphite dianion; PGH, phosphoglycolohydroxamate; L6RM, loop 6 replacement mutant; NADH, nicotinamide adenine dinucleotide, reduced form; NAD$^+$, nicotinamide adenine dinucleotide, oxidized form; NMR, nuclear magnetic resonance; OMPDC, orotidine 5′-monophosphate decarboxylase; G3P, glycerol 3-phosphate.

■ REFERENCES

(1) Fothergill-Gilmore, L. A. (1986) The evolution of the glycolytic pathway. *Trends Biochem. Sci. 11*, 47−51.

(2) Knowles, J. R., and Albery, W. J. (1977) Perfection in enzyme catalysis: The energetics of triosephosphate isomerase. *Acc. Chem. Res. 10*, 105−111.

(3) Knowles, J. R. (1991) To build an enzyme. *Philos. Trans. R. Soc. London, Ser. B 332*, 115−121.

(4) Waley, S. G., Miller, J. C., Rose, I. A., and O'Connell, E. L. (1970) Identification of site in triose phosphate isomerase labeled by glycidol phosphate. *Nature 227*, 181.

(5) De la Mare, S., Coulson, A. F. W., Knowles, J. R., Priddle, J. D., and Offord, R. E. (1972) Active-site labeling of triose phosphate isomerase. Reaction of bromohydroxyacetone phosphate with a unique glutamic acid residue and the migration of the label to tyrosine. *Biochem. J. 129*, 321−331.

(6) Straus, D., Raines, R., Kawashima, E., Knowles, J. R., and Gilbert, W. (1985) Active site of triosephosphate isomerase: In vitro mutagenesis and characterization of an altered enzyme. *Proc. Natl. Acad. Sci. U.S.A. 82*, 2272−2276.

(7) Zhang, Z., Komives, E. A., Sugio, S., Blacklow, S. C., Narayana, N., Xuong, N. H., Stock, A. M., Petsko, G. A., and Ringe, D. (1999) The Role of Water in the Catalytic Efficiency of Triosephosphate Isomerase. *Biochemistry 38*, 4389−4397.

(8) Malabanan, M. M., Nitsch-Velasquez, L., Amyes, T. L., and Richard, J. P. (2013) Magnitude and origin of the enhanced basicity of the catalytic glutamate of triosephosphate isomerase. *J. Am. Chem. Soc. 135*, 5978−5981.

(9) Lodi, P. J., and Knowles, J. R. (1991) Neutral imidazole is the electrophile in the reaction catalyzed by triosephosphate isomerase: Structural origins and catalytic implications. *Biochemistry 30*, 6948−6956.

(10) Komives, E. A., Chang, L. C., Lolis, E., Tilton, R. F., Petsko, G. A., and Knowles, J. R. (1991) Electrophilic catalysis in triosephosphate isomerase: The role of histidine-95. *Biochemistry 30*, 3011−3019.

(11) Nickbarg, E. B., Davenport, R. C., Petsko, G. A., and Knowles, J. R. (1988) Triosephosphate isomerase: Removal of a putatively electrophilic histidine residue results in a subtle change in catalytic mechanism. *Biochemistry 27*, 5948−5960.

(12) Wise, E., Yew, W. S., Babbitt, P. C., Gerlt, J. A., and Rayment, I. (2002) Homologous $(\beta/\alpha)_8$-Barrel Enzymes That Catalyze Unrelated Reactions: Orotidine 5′-Monophosphate Decarboxylase and 3-Keto-L-Gulonate 6-Phosphate Decarboxylase. *Biochemistry 41*, 3861−3869.

(13) Nagano, N., Orengo, C. A., and Thornton, J. M. (2002) One fold with many functions: The evolutionary relationships between TIM barrel families based on their sequences, structures and functions. *J. Mol. Biol. 321*, 741−765.

(14) Wierenga, R. K. (2001) The TIM-barrel fold: A versatile framework for efficient enzymes. *FEBS Lett. 492*, 193−198.

(15) Malabanan, M. M., Amyes, T. L., and Richard, J. P. (2010) A role for flexible loops in enzyme catalysis. *Cur. Opin. Struct. Biol. 20*, 702−710.

(16) Richard, J. P., Amyes, T. L., Goryanova, B., and Zhai, X. (2014) Enzyme architecture: On the importance of being in a protein cage. *Curr. Opin. Chem. Biol. 21*, 1−10.

(17) Richard, J. P. (2012) A Paradigm for Enzyme-Catalyzed Proton Transfer at Carbon: Triosephosphate Isomerase. *Biochemistry 51*, 2652−2661.

(18) Amyes, T. L., and Richard, J. P. (2013) Specificity in Transition State Binding: The Pauling Model Revisited. *Biochemistry 52*, 2021−2035.

(19) Amyes, T. L., Richard, J. P., and Tait, J. J. (2005) Activation of orotidine 5′-monophosphate decarboxylase by phosphite dianion: The whole substrate is the sum of two parts. *J. Am. Chem. Soc. 127*, 15708−15709.

(20) Goryanova, B., Amyes, T. L., Gerlt, J. A., and Richard, J. P. (2011) OMP Decarboxylase: Phosphodianion Binding Energy Is Used To Stabilize a Vinyl Carbanion Intermediate. *J. Am. Chem. Soc. 133*, 6545−6548.

(21) Tsang, W.-Y., Amyes, T. L., and Richard, J. P. (2008) A substrate in pieces: Allosteric activation of glycerol 3-phosphate dehydrogenase (NAD$^+$) by phosphite dianion. *Biochemistry 47*, 4575−4582.

(22) Ray, W. J., Jr., Long, J. W., and Owens, J. D. (1976) An analysis of the substrate-induced rate effect in the phosphoglucomutase system. *Biochemistry 15*, 4006−4017.

(23) Kholodar, S. A., and Murkin, A. S. (2013) DXP Reductoisomerase: Reaction of the Substrate in Pieces Reveals a Catalytic Role for the Nonreacting Phosphodianion Group. *Biochemistry 52*, 2302−2308.

(24) Wierenga, R. K. (2010) Triosephosphate isomerase: A highly evolved biocatalyst. *Cell. Mol. Life Sci. 67*, 3961−3982.

(25) Samanta, M., Murthy, M. R. N., Balaram, H., and Balaram, P. (2011) Revisiting the Mechanism of the Triosephosphate Isomerase Reaction: The Role of the Fully Conserved Glutamic Acid 97 Residue. *ChemBioChem 12*, 1886−1895.

(26) Go, M. K., Amyes, T. L., and Richard, J. P. (2010) Rescue of K12G mutant TIM by NH$_4^+$ and alkylammonium cations: The reaction of an enzyme in pieces. *J. Am. Chem. Soc. 132*, 13525−13532.

(27) Go, M. K., Koudelka, A., Amyes, T. L., and Richard, J. P. (2010) Role of Lys-12 in Catalysis by Triosephosphate Isomerase: A Two-Part Substrate Approach. *Biochemistry 49*, 5377−5389.

(28) Pompliano, D. L., Peyman, A., and Knowles, J. R. (1990) Stabilization of a reaction intermediate as a catalytic device: Definition of the functional role of the flexible loop in triosephosphate isomerase. *Biochemistry 29*, 3186−3194.

(29) Richard, J. P. (1993) Mechanism for the formation of methylgloxal from triosephosphates. *Biochem. Soc. Trans. 21*, 549−553.

(30) Richard, J. P. (1991) Kinetic-parameters for the elimination reaction catalyzed by triosephosphate isomerase and an estimation of the reactions physiological significance. *Biochemistry 30*, 4581−4585.

(31) Richard, J. P. (1984) Acid-base catalysis of the elimination and isomerization reactions of triose phosphates. *J. Am. Chem. Soc. 106*, 4926−4936.

(32) Amyes, T. L., and Richard, J. P. (2007) Enzymatic catalysis of proton transfer at carbon: Activation of triosephosphate isomerase by phosphite dianion. *Biochemistry 46*, 5841−5854.

(33) Go, M. K., Amyes, T. L., and Richard, J. P. (2009) Hydron Transfer Catalyzed by Triosephosphate Isomerase. Products of the Direct and Phosphite-Activated Isomerization of [1-^{13}C]-Glycolaldehyde in D$_2$O. *Biochemistry 48*, 5769−5778.

(34) Goryanova, B., Spong, K., Amyes, T. L., and Richard, J. P. (2013) Catalysis by Orotidine 5′-Monophosphate Decarboxylase: Effect of 5-Fluoro and 4′-Substituents on the Decarboxylation of Two-Part Substrates. *Biochemistry 52*, 537−546.

(35) Amyes, T. L., Ming, S. A., Goldman, L. M., Wood, B. M., Desai, B. J., Gerlt, J. A., and Richard, J. P. (2012) Orotidine 5′-monophosphate decarboxylase: Transition state stabilization from remote protein-phosphodianion interactions. *Biochemistry 51*, 4630−4632.

(36) Joseph, D., Petsko, G. A., and Karplus, M. (1990) Anatomy of a conformational change: Hinged "lid" motion of the triosephosphate isomerase loop. *Science 249*, 1425−1428.

(37) Xu, Y., Lorieau, J., and McDermott, A. E. (2010) Triosephosphate isomerase: ^{15}N and ^{13}C chemical shift assignments and conformational change upon ligand binding by magic-angle spinning solid-state NMR spectroscopy. *J. Mol. Biol. 397*, 233−248.

(38) Rozovsky, S., and McDermott, A. E. (2001) The time scale of the catalytic loop motion in triosephosphate isomerase. *J. Mol. Biol. 310*, 259−270.

(39) Rozovsky, S., Jogl, G., Tong, L., and McDermott, A. E. (2001) Solution-state NMR investigations of triosephosphate isomerase active site loop motion: Ligand release in relation to active site loop dynamics. *J. Mol. Biol. 310*, 271−280.

(40) Massi, F., Wang, C., and Palmer, A. G., III (2006) Solution NMR and computer simulation studies of active site loop motion in triosephosphate isomerase. *Biochemistry 45*, 10787−10794.

(41) Berlow, R. B., Igumenova, T. I., and Loria, J. P. (2007) Value of a Hydrogen Bond in Triosephosphate Isomerase Loop Motion. *Biochemistry 46*, 6001−6010.

(42) Desamero, R., Rozovsky, S., Zhadin, N., McDermott, A., and Callender, R. (2003) Active site loop motion in triosephosphate isomerase: T-Jump relaxation spectroscopy of thermal activation. *Biochemistry 42*, 2941−2951.

(43) Sun, J., and Sampson, N. S. (1999) Understanding protein lids: Kinetic analysis of active hinge mutants in triosephosphate isomerase. *Biochemistry 38*, 11474−11481.

(44) Sun, J., and Sampson, N. S. (1998) Determination of the amino acid requirements for a protein hinge in triosephosphate isomerase. *Protein Sci. 7*, 1495−1505.

(45) Kempf, J. G., Jung, J.-y., Ragain, C., Sampson, N. S., and Loria, J. P. (2007) Dynamic requirements for a functional protein hinge. *J. Mol. Biol. 368*, 131−149.

(46) Xiang, J., Jung, J.-y., and Sampson, N. S. (2004) Entropy effects on protein hinges: The reaction catalyzed by triosephosphate isomerase. *Biochemistry 43*, 11436−11445.

(47) Kursula, I., Salin, M., Sun, J., Norledge, B. V., Haapalainen, A. M., Sampson, N. S., and Wierenga, R. K. (2004) Understanding protein lids: Structural analysis of active hinge mutants in triosephosphate isomerase. *Protein Eng., Des. Sel. 17*, 375−382.

(48) O'Donoghue, A. C., Amyes, T. L., and Richard, J. P. (2008) Slow proton transfer from the hydrogen-labelled carboxylic acid side chain (Glu-165) of triosephosphate isomerase to imidazole buffer in D_2O. *Org. Biomol. Chem. 6*, 391−396.

(49) O'Donoghue, A. C., Amyes, T. L., and Richard, J. P. (2005) Hydron Transfer Catalyzed by Triosephosphate Isomerase. Products of Isomerization of Dihydroxyacetone Phosphate in D_2O. *Biochemistry 44*, 2622−2631.

(50) O'Donoghue, A. C., Amyes, T. L., and Richard, J. P. (2005) Hydron Transfer Catalyzed by Triosephosphate Isomerase. Products of Isomerization of (R)-Glyceraldehyde 3-Phosphate in D_2O. *Biochemistry 44*, 2610−2621.

(51) O'Connor, E. J., Tomita, Y., and McDermott, A. E. (1994) Synthesis of $(1,2-^{13}C_2)$-2-phosphoglycolic acid. *J. Labelled Compd. Radiopharm. 34*, 735−740.

(52) Bergemeyer, H. U., Haid, E., and Nelboeck-Hochstetter, M. (1972) Process for preparing open ring tetrose and triosephosphate acetals and phosphate ketals. U.S. Patent 3,662,037.

(53) Zhai, X., Amyes, T. L., Wierenga, R. K., Loria, J. P., and Richard, J. P. (2013) Structural Mutations That Probe the Interactions between the Catalytic and Dianion Activation Sites of Triosephosphate Isomerase. *Biochemistry 52*, 5928−5940.

(54) Desai, K. K., and Miller, B. G. (2008) A Metabolic Bypass of the Triosephosphate Isomerase Reaction. *Biochemistry 47*, 7983−7985.

(55) Gasteiger, E., Hoogland, C., Gattiker, A., Duvaud, S., Wilkins, M. R., Appel, R. D., and Bairoch, A. (2005) Protein identification and analysis tools on the ExPASy server. *Proteomics Protoc. Handb.*, 571−607.

(56) Hermes, J. D., Parekh, S. M., Blacklow, S. C., Koster, H., and Knowles, J. R. (1989) A reliable method for random mutagenesis: The generation of mutant libraries using spiked oligodeoxyribonucleotide primers. *Gene 84*, 143−151.

(57) Straus, D., and Gilbert, W. (1985) Chicken triosephosphate isomerase complements an *Escherichia coli* deficiency. *Proc. Natl. Acad. Sci. U.S.A. 82*, 2014−2018.

(58) Otwinowski, Z., and Minor, W. (1997) *Processing of X-ray Diffraction Data Collected in Oscillation Mode*, Macromolecular Crystallography, Part A, Vol. 276, Academic Press, New York.

(59) Zhang, Z., Sugio, S., Komives, E. A., Liu, K. D., Knowles, J. R., Petsko, G. A., and Ringe, D. (1994) Crystal structure of recombinant chicken triosephosphate isomerase-phosphoglycolohydroxamate complex at 1.8-Å resolution. *Biochemistry 33*, 2830−2837.

(60) Bailey, S. (1994) The CCP4 Suite: Programs for Protein Crystallography. *Acta Crystallogr. D50*, 760−763.

(61) Delaglio, F., Grzesiek, S., Vuister, G., Zhu, G., Pfeifer, J., and Bax, A. (1995) NMRPipe: A multidimensional spectral processing system based on UNIX pipes. *J. Biomol. NMR 6*, 277−293.

(62) Goddard, T., and Kneller, D. G. (2010) *SPARKY 3*, University of California, San Francisco.

(63) Loria, J. P., Rance, M., and Palmer, A., III (1999) A TROSY CPMG sequence for characterizing chemical exchange in large proteins. *J. Biomol. NMR 15*, 151−155.

(64) Loria, J. P., Rance, M., and Palmer, A. G., III (1999) Transverse-Relaxation-Optimized (TROSY) Gradient-Enhanced Triple-Resonance NMR Spectroscopy. *J. Magn. Reson. 141*, 180−184.

(65) Wittekind, M., and Mueller, L. (1993) HNCACB, a High-Sensitivity 3D NMR Experiment to Correlate Amide-Proton and Nitrogen Resonances with the α- and β-Carbon Resonances in Proteins. *J. Magn. Reson., Ser. B 101*, 201−205.

(66) Kay, L. E., Ikura, M., Tschudin, R., and Bax, A. (1990) 3-Dimensional Triple-Resonance NMR-Spectroscopy of Isotopically Enriched Proteins. *J. Magn. Reson. 89*, 496−514.

(67) Grzesiek, S., Stahl, S. J., Wingfield, P. T., and Bax, A. (1996) The CD4 Determinant for Downregulation by HIV-1 Nef Directly Binds to Nef. Mapping of the Nef Binding Surface by NMR. *Biochemistry 35*, 10256−10261.

(68) Hernandez-Alcantara, G., Rodriguez-Romero, A., Reyes-Vivas, H., Peon, J., Cabrera, N., Ortiz, C., Enriquez-Flores, S., De la Mora-De la Mora, I., and Lopez-Velazquez, G. (2008) Unraveling the mechanisms of tryptophan fluorescence quenching in the triosephosphate isomerase from *Giardia lamblia*. *Biochim. Biophys. Acta 1784*, 1493−1500.

(69) Nickbarg, E. B., and Knowles, J. R. (1988) Triosephosphate isomerase: Energetics of the reaction catalyzed by the yeast enzyme expressed in *Escherichia coli*. *Biochemistry 27*, 5939−5947.

(70) Wolfenden, R. (1969) Transition state analogues for enzyme catalysis. *Nature 223*, 704−705.

(71) Malabanan, M. M., Koudelka, A. P., Amyes, T. L., and Richard, J. P. (2012) Mechanism for Activation of Triosephosphate Isomerase by Phosphite Dianion: The Role of a Hydrophobic Clamp. *J. Am. Chem. Soc. 134*, 10286−10298.

(72) Malabanan, M. M., Go, M., Amyes, T. L., and Richard, J. P. (2011) Wildtype and Engineered Monomeric Triosephosphate Isomerase from *Trypanosoma brucei*: Partitioning of Reaction Intermediates in D_2O and Activation by Phosphite Dianion. *Biochemistry 50*, 5767−5679.

(73) Malabanan, M. M., Amyes, T. L., and Richard, J. P. (2011) Mechanism for Activation of Triosephosphate Isomerase by Phosphite

Dianion: The Role of a Ligand-Driven Conformational Change. *J. Am. Chem. Soc. 133*, 16428−16431.

(74) Go, M. K., Malabanan, M. M., Amyes, T. L., and Richard, J. P. (2010) Bovine Serum Albumin-Catalyzed Deprotonation of [1-^{13}C]-Glycolaldehyde: Protein Reactivity toward Deprotonation of the α-Hydroxy α-Carbonyl Carbon. *Biochemistry 49*, 7704−7708.

(75) Kursula, I., Salin, M., Sun, J., Norledge, B. V., Haapalainen, A. M., Sampson, N. S., and Wierenga, R. K. (2004) Understanding protein lids: Structural analysis of active hinge mutants in triosephosphate isomerase. *Protein Eng., Des. Sel. 17*, 375−382.

(76) Dougherty, D. A. (2013) The Cation-π Interaction. *Acc. Chem. Res. 46*, 885−893.

(77) Walden, H., Taylor, G., Lilie, H., Knura, T., and Hensel, R. (2004) Triosephosphate isomerase of the hyperthermophile *Thermoproteus tenax*: Thermostability is not everything. *Biochem. Soc. Trans. 32*, 305−305.

(78) Walden, H., Bell, G. S., Russell, R. J. M., Siebers, B., Hensel, R., and Taylor, G. L. (2001) Tiny TIM: A small, tetrameric, hyperthermostable triosephosphate isomerase. *J. Mol. Biol. 306*, 745−757.

(79) Gayathri, P., Banerjee, M., Vijayalakshmi, A., Azeez, S., Balaram, H., Balaram, P., and Murthy, M. R. N. (2007) Structure of triosephosphate isomerase (TIM) from *Methanocaldococcus jannaschii*. *Acta Crystallogr. D63*, 206−220.

(80) Xiang, J., Sun, J., and Sampson, N. S. (2001) The importance of hinge sequence for loop function and catalytic activity in the reaction catalyzed by triosephosphate isomerase. *J. Mol. Biol. 307*, 1103−1112.

(81) Zhai, X., Malabanan, M. M., Amyes, T. L., and Richard, J. P. (2014) Mechanistic imperatives for deprotonation of carbon catalyzed by triosephosphate isomerase: Enzyme activation by phosphite dianion. *J. Phys. Org. Chem. 27*, 269−276.

(82) Zhai, X., Amyes, T. L., and Richard, J. P. (2014) Enzyme Architecture: Remarkably Similar Transition States for Triosephosphate Isomerase-Catalyzed Reactions of the Whole Substrate and the Substrate in Pieces. *J. Am. Chem. Soc. 136*, 4145−4148.

(83) Lolis, E., and Petsko, G. A. (1990) Crystallographic analysis of the complex between triosephosphate isomerase and 2-phosphoglycolate at 2.5-Å resolution: Implications for catalysis. *Biochemistry 29*, 6619−6625.